Mathematical Modelling and Control

https://www.aimspress.com/journal/mmc

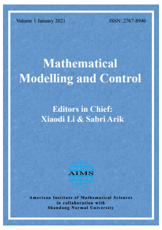

MMC, 6(2): 163–184.
DOI: 10.3934/mmc.2026013
Received: 24 December 2024
Revised: 28 May 2025
Accepted: 06 August 2025
Published: 08 June 2026

Research article

Enhanced LMI-Based composite nonlinear control for a knee rehabilitation exoskeleton robot considering motion constraints

Sahar Jenhani[1], **Hassène Gritli**[1,2,*] **and Jyotindra Narayan**[3]

[1] Laboratory of Robotics, Informatics and Complex Systems (RISC Lab - LR16ES07), National Engineering School of Tunis, University of Tunis El Manar, BP. 37, Le Belvédère, 1002, Tunis, Tunisia

[2] Higher Institute of Information and Communication Technologies, University of Carthage, Technopole of Borj Cédria, Route de Soliman, BP 123, Hammam Chatt 1164, Ben Arous, Tunisia

[3] Department of Mechanical Engineering, Indian Institute of Technology Patna, Patna 801106, India

* **Correspondence:** Email: grhass@yahoo.fr.

Abstract: This paper proposes a novel robust control strategy for the stabilization of a knee rehabilitation exoskeleton robot. Unlike traditional methods, the designed controller combines a linear state-feedback law with a nonlinear compensation term to effectively address the robot's nonlinear dynamics under parameter uncertainties, external disturbances, and motion constraints. Two complementary approaches are introduced: one assumes a constant bound on the nonlinearities and another employs a state-dependent linear constraint. For each approach, tailored Linear Matrix Inequality (LMI) conditions are derived using specific technical lemmas, including Young's inequality, the S-procedure, the Schur complement, and the matrix inversion lemma. The originality of this work lies in the systematic integration of motion constraints and external disturbances into the LMI framework for composite control. Numerical simulations validate the proposed methodology, thereby demonstrating superior robustness and stability performance compared to conventional control strategies.

Keywords: knee exoskeleton robot; robust position control; composite controller; motion constraints; linear matrix inequality (LMI)

1. Introduction

The increasing demand for advanced rehabilitation technologies has spurred extensive research in the field of robotic exoskeletons, particularly those designed to assist individuals with mobility impairments [1–3]. These wearable robotic devices are instrumental in addressing the mobility challenges faced by aging populations and patients recovering from neurological conditions, such as spinal cord injuries or strokes [3–6]. Exoskeletons provide vital support for walking, balance, and other daily activities, offering a promising solution to enhance physical rehabilitation and improve the quality of life [7]. Among these devices, lower limb exoskeletons, especially those which focus on the knee joint, are critical due to the central role this joint plays in weight-bearing and locomotion [8, 9]. Effective control systems are key to ensuring the safe and precise operation of these exoskeletons during rehabilitation, thus enabling patients to regain mobility and independence [10].

Control systems for knee-joint exoskeletons must overcome several technical challenges, including the management of nonlinear dynamics, parameter uncertainties, and external disturbances such as friction. These complexities arise from the intrinsic characteristics of the knee joint's motion, which not only involves rotational dynamics but also interactions with the environment and human body [10–12]. Additionally, the presence of viscous and solid friction, along with external disturbances, further complicates the control design process. In this context, ensuring robust and adaptive control of the exoskeleton is crucial to offer patients with smooth and stable assistance throughout rehabilitation exercises [8–10, 13].

In recent years, significant advancements have been made in the development of control strategies for knee exoskeletons, particularly aimed at improving rehabilitation for individuals with spinal cord injuries and other lower limb disabilities. For instance, [14] proposed a hybrid control strategy which combined Active Disturbance Rejection Control (ADRC) with Sliding Mode Control (SMC), effectively addressing both disturbances and nonlinearities inherent in lower limb exoskeleton systems. This innovative approach demonstrated superior disturbance rejection and tracking performance compared to traditional control methods. Similarly, authors in [15] implemented ADRC for knee-joint exoskeletons, thereby leveraging extended state observers (ESO) to estimate disturbances and enhance the system's robustness against parameter variations, significantly outperforming conventional control schemes in terms of thr stability and adaptability. Moreover, a study by [16] highlighted the benefits of ADRC in controlling both the hip and knee joints during rehabilitation, showing improved precision and stability in tracking compared to standard proportional-derivative controllers. This research emphasized the critical role of ESO in managing system uncertainties. Building upon these advancements, [17] introduced an error-based ADRC (EADRC), which alleviates the challenges associated with derivative actions in traditional ADRC schemes. Their results demonstrated that EADRC outperforms conventional ADRC in terms of the tracking accuracy, noise rejection, and handling load uncertainties, further advancing the efficiency of knee rehabilitation exoskeletons. Parallel to these efforts, other significant contributions have focused on refining control techniques for knee exoskeletons. To address the nonlinear dynamic model of the knee-joint rehabilitation exoskeleton, which includes complexities such as viscous and solid friction, an affine state-feedback control law was also explored [18]. State-feedback control methods have consistently shown their effectiveness in regulating knee joint movements in lower limb orthoses, as evidenced by various studies [19]. Moreover, a composite control strategy that combines linear state-feedback with nonlinear control was developed to achieve robust stabilization [19]. Other advanced control techniques include the adaptive RISE controller proposed in [20] to handle the high nonlinearities inherent in exoskeleton control, specifically designed for the EICoSI knee exoskeleton. Additionally, [12] introduced a non-singular terminal sliding mode approach for active orthosis control, while [11] utilized an adaptive control law based on radial basis function neural networks to operate a motorized knee orthosis. More recently, online adaptive PID controllers optimized through the particle swarm optimization (PSO) algorithm for multi-joint exoskeletons were developed [21], and a model reference adaptive control (MRAC) strategy was proposed to control the angular position of an exoskeleton knee assistance system [22]. Additionally, fuzzy PID control was investigated for actuated exoskeleton systems [23]. Comprehensive surveys, such as those provided in [24], offer an overview of lower-limb orthoses powered by pneumatic muscle-type actuators, while works such as [25, 26] thoroughly examined the classification, design, and control methods of lower-limb rehabilitation robots (LLRERs). Recent reviews on gait assistance devices, including [27–30], offer valuable insights into the performance evaluation of these devices. However, while these reviews present broad perspectives on the development and functionality of assistive devices, they often lack detailed discussions on the specific control strategies required for robust, real-world exoskeleton operation, especially in the context of fully mobilizing systems. Although some studies, such as [28], focused on aspects such as metabolic cost reduction, they do not sufficiently address the underlying control mechanisms necessary to ensure stability and robustness under uncertain operating conditions.

Despite substantial advancements, several important limitations in the current literature have motivated the present study. For example, Alawad et al. [14] proposed a hybrid ADRC-SMC controller that enhances robustness and reduces chattering, yet it did not explicitly address state constraints. Similarly, Al et al. [15] compared LESO- and NESO-based ADRC variants, thereby demonstrating improved disturbance rejection, but overlooked joint limitations. In another work, Alawad et al. [16] focused on controlling hip and knee coordination using ADRC, thereby effectively mitigating dynamic coupling but without handling state constraints. Alawad et al. [17] introduced an error-based ADRC formulation to reduce noise sensitivity and improve load rejection, though it remains limited in robustness under parametric uncertainties. Although adaptive nonlinear controls such as RISE [20] have addressed certain classes of disturbances, they often lack a systematic treatment of parameter variations and constraints. Composite control strategies have also been proposed [31], but many rely on simplified nonlinear models and do not fully ensure robustness or control efficiency in constrained conditions. Similarly, while state-feedback and affine PD controllers [18] have shown promising tracking performance, their integration of uncertainty management and constraint enforcement remains limited. Lastly, although Linear Matrix Inequality (LMI)-based methods offer rigorous stability guarantees, their systematic deployment in robust exoskeleton control is still underexplored. These gaps highlight the need for more comprehensive control frameworks that explicitly ensure robustness, adaptability, and safety in the presence of real-world uncertainties and physical joint limitations.

Motivated by these challenges, this study presents an effective control strategy designed for the robust stabilization of a 1-DoF knee rehabilitation exoskeleton robot [18,19,31]. Focused on position control, the proposed approach systematically addresses various challenges, including state constraints, parameter uncertainties, solid and viscous frictions, and external disturbances. The developed control scheme integrates a linear state-feedback controller with a nonlinear control law, formulated to effectively manage the complex dynamics and uncertainties inherent in knee-joint exoskeleton systems. The nonlinear functions present in the dynamics of the knee exoskeleton are approximated under two different assumptions. Initially, the nonlinearities are considered to be bounded by a constant, thus leading to the development of the first design approach to formulate LMI conditions. Subsequently, the nonlinear functions are treated as being constrained by a linear equation, resulting in the second LMI-based design method. LMI criteria for the feedback gains of the controller are established from a quadratic Lyapunov function, which ensures the stability and robustness of the suggested control technique. These conditions are formulated using a theoretical framework that incorporates several technical lemmas, including Young's inequality, the matrix inversion lemma, the Schur complement, and the S-procedure [19]. To validate the effectiveness of the developed approaches, simulations are conducted that introduce external disturbances and examine the system's performance. The results demonstrate that the control system successfully stabilizes the knee-joint exoskeleton, thus ensuring robust position control despite the nonlinearities and external forces which act on the system. A comparison of the developed control strategies is carried out to evaluate their effectiveness, thereby aiming to identify the most optimal approach for various conditions.

The following outlines the main contributions of this study:

- Introduction of a novel composite control strategy, thereby combining a linear state-feedback controller with a nonlinear control law to stabilize a 1-DoF knee rehabilitation exoskeleton robot. This strategy effectively addresses nonlinear dynamics, state constraints, frictions, and external disturbances, ensuring robust performances under parameter uncertainties.
- Derivation of LMI-based conditions to determine the controller's feedback gain, using a quadratic Lyapunov function to guarantee stability and robustness. The theoretical framework incorporates key lemmas such as Young's inequality, the Schur complement, and the matrix inversion lemma.
- Validation of the proposed control strategy through numerical simulations, demonstrating its effectiveness in stabilizing the exoskeleton under disturbances, thereby uncertainties, and complex dynamic behaviors.
- Comparative analysis of control strategies, thereby evaluating multiple approaches and highlighting the advantages of the proposed method in terms of stability, disturbance rejection, and control performance.

The structure of this paper is outlined as follows: the dynamic modeling of the knee exoskeleton is presented in Section 2; in Section 3, the focus shifts to the development of a robust control strategy tailored for the exoskeleton; in

Section 4 discusses the derivation of stability conditions using the LMI-based approach; simulation results that evaluate the controller's effectiveness are presented in Section 5; and lastly, Section 6 provides concluding insights and suggests avenues for future work.

2. Modeling the nonlinear dynamics of the knee exoskeleton

2.1. Overview of the knee-joint exoskeleton

This study focuses on wearable exoskeletons that operate in the sagittal plane, distinguishing three joint conditions: fixed, active, or with 1-DoF per leg. Our primary aim is to precisely control the position, specifically at the knee-joint level, for a powered lower-limb exoskeleton system [32]. Exoskeletons with 1-DoF are particularly well-suited for applications that require support or rehabilitation for specific movements [8, 11, 22, 32]. The robotic exoskeleton shown in Figure 1 incorporates a 1-DoF knee joint, which was chosen for its user-friendly and simple design, thus aligning with the goals of this research. This streamlined design makes it especially appropriate for individuals with knee joint impairments [32].

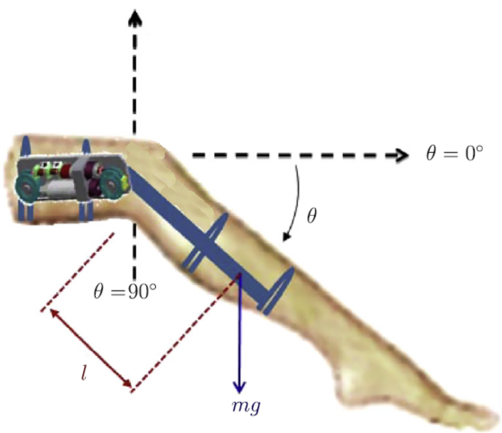

Figure 1. The selected 1-DoF knee rehabilitation exoskeleton [18, 19, 32].

One of the key advantages of 1-DoF exoskeletons is their versatility across various practical applications. In rehabilitation, they play a crucial role in strengthening muscles and enhancing mobility. In industrial settings, they assist in lifting heavy loads, thus reducing the risk of injury. Additionally, they enhance the quality of life for individuals with gait impairments by facilitating walking and reducing muscle fatigue for both workers and athletes. For elderly or disabled individuals, they also provide essential support in daily tasks, such as standing up or climbing stairs.

2.2. Dynamic representation of leg-orthosis interaction

Using a pendulum model to represent the exoskeleton robot, we can derive its dynamic model using the Lagrangian mechanical system [19, 31], which results in the following equations of motion:

$$\frac{d}{dt}\left(\frac{\partial \mathcal{L}}{\partial \dot{\theta}}\right) - \frac{\partial \mathcal{L}}{\partial \theta} = \mathcal{T}. \tag{2.1}$$

In this context, T, which represents total torques acting on the robot, is defined by the following equation:

$$\mathcal{T} = -\mathcal{T}_s - \mathcal{T}_v - \delta_t + u, \tag{2.2}$$

where

- $\mathcal{T}_v = f_v\dot{\theta}$ indicates the torque related to viscous friction,
- $\mathcal{T}_s = f_s\text{sgn}(\dot{\theta})$ corresponds to the torque due to solid friction,
- δ_t represents the load torque, and
- u denotes the control torque applied to the system.

In Eq (2.1), $\mathcal{L}$ refers to the Lagrangian function, which is described as follows:

$$\mathcal{L} = -\mathcal{G}_e + \mathcal{K}_e, \tag{2.3}$$

where $\mathcal{G}_e$ denotes the gravitational potential energy, and $\mathcal{K}_e$ denotes the kinetic energy.

By inserting Eqs (2.2) and (2.3) into the Lagrangian equation (2.1), we derive the dynamics of the knee exoskeleton depicted in Figure 1, thereby considering uncertainties including external disturbances, unmodeled dynamics, and parameter variations, as follows:

$$\vartheta\ddot{\theta} = -f_s\text{sgn}(\dot{\theta}) - f_v\dot{\theta} + a\cos(\theta) + \delta_t + u. \tag{2.4}$$

Here, ϑ represents the exoskeleton's moment of inertia, f_v represents the viscous friction coefficient, f_s represents the solid friction coefficient, and $a = mgl$, with m being the mass, l representing the length, and g representing the gravitational constant.

In previous work, the authors rely on a nonlinear dynamic model that does not account for uncertainties. In contrast, this present work separates the system dynamics into a nominal component and an uncertain component, which allows for a more accurate representation of the variability in the system behavior [19, 31]. This separation provides a clearer understanding of the sources of uncertainty, thus leading to a more robust controller design. The system's parameters are defined as follows:

$$a = a_\star + \Delta a, \qquad \vartheta = \vartheta_\star + \Delta\vartheta,$$
$$f_v = f_v^\star + \Delta f_v, \quad \text{and} \quad f_s = f_s^\star + \Delta f_s. \tag{2.5}$$

Substituting these parameters into the nonlinear dynamics Eq (2.4) results in the following model:

$$\vartheta_\star \ddot{\theta} = a_\star \cos(\theta) - f_s^\star \mathrm{sgn}(\dot{\theta}) - f_v^\star \dot{\theta} + u + \Delta_t, \tag{2.6}$$

where the total disturbance Δ_t is defined as follows:

$$\Delta_t = \delta_t - \Delta\vartheta\ddot{\theta} + \Delta a \cos(\theta) - \Delta f_s \mathrm{sgn}(\dot{\theta}) - \Delta f_v \dot{\theta}. \tag{2.7}$$

In the subsequent analysis, we assume that Δ_t satisfies the following constraint:

$$|\Delta_t| \leq \bar{\delta}, \qquad \text{where} \qquad \bar{\delta} > 0. \tag{2.8}$$

By introducing the variable $\phi = \theta - \theta_d$, with θ_d signifying the target position of the knee joint, the dynamic model (2.4) is rewritten as follows:

$$\vartheta_\star \ddot{\phi} = -f_v^\star \dot{\phi} + \Delta_t + u - f_s^\star \mathrm{sgn}(\dot{\phi}) + a_\star \cos(\phi + \theta_d). \tag{2.9}$$

To maintain the exoskeleton at the equilibrium position ($\dot{\theta}_d = 0$) with a steady control effort after positioning it at the desired angle θ_d, let u_d represent the required equilibrium control torque. From Eq (2.9), we have the following:

$$0 = u_d + a_\star \cos(\theta_d). \tag{2.10}$$

Thus, the required equilibrium control effort u_d is given by the following:

$$u_d = -a_\star \cos(\theta_d). \tag{2.11}$$

3. Designing a robust control approach for the knee exoskeleton

3.1. Formulation of the research problem

Advancements in technology have led to the emergence of exoskeleton robots as versatile devices that support mobility and rehabilitation tailored to individual needs. Researchers have explored various control strategies to ensure robust position control in exoskeleton systems, particularly for lower limb rehabilitation, while prioritizing safety and an adherence to motion constraints [32, 33].

In previous work [18], the focus was on the general control of the exoskeleton without accounting for these constraints, which may be acceptable in some cases but does not guarantee a safe and optimal operation under all conditions. By incorporating motion constraints, the current design improves both the safety and efficiency of the system, thus preventing excessive forces or incorrect movements. The inclusion of motion constraints in the controller design serves several important objectives. First, it ensures that the controller operates within the physical limits of the knee joint, thereby preventing overextension or excessive bending, which could lead to damage or reduced performance of the exoskeleton. By explicitly considering these constraints, the controller can adapt to the system's inherent limitations, thus ensuring a safer and more efficient operation, especially in practical applications.

In this work, we explicitly consider these constraints to ensure that the controller operates within the physical limitations of the system [31]. This study focuses on the exoskeleton robotic system at the knee joint, which functions within a range of 90°, as illustrated in Figure 1. Here, the knee joint is fully extended at 0° and at rest at 90°. The set Ω defines the operational range of the knee exoskeleton in the following manner:

$$\Omega = \{\theta \in \mathbb{R} : 0 \leq \theta \leq \frac{\pi}{2}\}. \tag{3.1}$$

In designing the controller u, it is essential to manage the nonlinear dynamics of the exoskeleton, represented by Eq (2.4) or Eq (2.9), while respecting the state constraint (3.1). Introducing the variable $\phi = \theta - \theta_d$ to represent the tracking error between the actual and desired knee positions, the state constraint can be reformulated as follows:

$$-\gamma_1 \leq \phi \leq \gamma_2, \tag{3.2}$$

where the scalars γ_1 and γ_2 are defined as follows:

$$\gamma_1 = \theta_d, \qquad \text{and} \qquad \gamma_2 = \frac{\pi}{2} - \theta_d. \tag{3.3}$$

Let $\mathcal{X} = \begin{bmatrix} \phi & \dot{\phi} \end{bmatrix}^{\mathrm{T}}$ be the state vector. Then, the dynamics (2.9) can be formulated as follows:

$$\begin{aligned} \dot{\mathcal{X}} =& \mathcal{A}\mathcal{X} + \mathcal{B}u + \mathcal{D}_1\Phi_1(\mathcal{X}) + \mathcal{D}_2\Phi_2(\mathcal{X}) + \mathcal{B}\Delta_t \\ &\text{with} \quad -\gamma_1 \leq C^{\mathrm{T}}\mathcal{X} \leq \gamma_2. \end{aligned} \tag{3.4}$$

The following defines $\Phi_1(\mathcal{X})$ and $\Phi_2(\mathcal{X})$:

$$\Phi_1(\mathcal{X}) = \mathrm{sgn}(\dot{\phi}), \tag{3.5}$$

$$\Phi_2(\mathcal{X}) = \cos(\phi + \theta_d). \tag{3.6}$$

The following specifies the matrices $\mathcal{A}$, $\mathcal{B}$, $\mathcal{D}1$, $\mathcal{D}2$, and C:

$$\begin{aligned} &\mathcal{A} = \begin{bmatrix} 0 & 1 \\ 0 & -\frac{f_v^\star}{\vartheta_\star} \end{bmatrix}, \quad \mathcal{B} = \begin{bmatrix} 0 \\ \frac{1}{\vartheta_\star} \end{bmatrix}, \qquad C = \begin{bmatrix} 1 \\ 0 \end{bmatrix}, \\ &\mathcal{D}_1 = \begin{bmatrix} 0 \\ -\frac{f_s^\star}{\vartheta_\star} \end{bmatrix}, \qquad \text{and} \quad \mathcal{D}_2 = \begin{bmatrix} 0 \\ \frac{a_\star}{\vartheta_\star} \end{bmatrix}. \end{aligned} \tag{3.7}$$

3.2. Composite control strategy and closed-loop modeling

The main goal of this work is to develop a controller that efficiently regulates and stabilizes the knee exoskeleton system at a specified position, θ_d. Consequently, the composite controller is formulated as follows:

$$u = u_{nl} + u_l. \tag{3.8}$$

In this formulation, the linear state feedback controller, denoted by u_l, is expressed as follows:

$$u_l = u_d + \Delta u_l. \tag{3.9}$$

The term u_d is defined according to Eq (2.11), while the term Δu_l is characterized as follows:

$$\Delta u_l = \mathcal{K}\mathcal{X}. \tag{3.10}$$

where $\mathcal{K}$ represents the gains matrix to be determined.

The term u_{nl} in Eq (3.8) corresponds to a nonlinear feedback controller, which will be subsequently defined. This additional controller is intended to mitigate the effects of external disturbances and friction.

Remark 3.1. *In this study, we propose a composite control strategy (3.8) that integrates a linear component u_l with a nonlinear component u_{nl}, each addressing specific control objectives. The linear term, defined in (3.9) with Δu_l specified in (3.10), provides basic stabilization toward the target state θ_d by applying state feedback to correct small deviations. The nonlinear term u_{nl} is designed to counteract disturbances Δ_t caused by nonlinear dynamics and external forces that could undermine the stability. Together, u_l and u_{nl} ensure robust stabilization and enhanced precision in the exoskeleton's position control.*

Substituting the composite control law (3.8) into the system dynamics (3.4) yields the following the closed-loop model:

$$\begin{aligned} &\dot{\mathcal{X}} = (\mathcal{A} + \mathcal{B}\mathcal{K})\mathcal{X} + \mathcal{B}\,u_{nl} + \mathcal{D}_1\Phi_1(\mathcal{X}) + \mathcal{D}_2\Phi_3(\mathcal{X}) + \mathcal{B}\Delta_t \\ &\quad \text{such that} \quad -\gamma_1 \leq C^{\mathrm{T}}\mathcal{X} \leq \gamma_2. \end{aligned} \tag{3.11}$$

The function $\Phi_3(\mathcal{X})$ is defined as follows:

$$\Phi_3(\mathcal{X}) = -\cos(\theta_d) + \cos(\phi + \theta_d). \tag{3.12}$$

4. Nonlinear controller design and LMI stability conditions

In this section, we outline two approaches to construct the nonlinear controller u_{nl} by utilizing the Lyapunov technique. Following this, we will design the linear state feedback component, denoted as Δu_l. Moreover, to determine the stability criteria needed to calculate the gain of the linear control element, we will apply the LMI framework. These LMI conditions are essential to ensure the stabilization of the exoskeleton robot.

To accomplish our objective, we will utilize a proposed Lyapunov function defined as follows:

$$\mathcal{V}(\mathcal{X}) = \mathcal{X}^{\mathrm{T}}\mathcal{P}\mathcal{X} \quad \text{such that} \quad -\gamma_1 \leq C^{\mathrm{T}}\mathcal{X} \leq \gamma_2. \tag{4.1}$$

The time derivative of this Lyapunov function is given by the following:

$$\dot{\mathcal{V}}(\mathcal{X}) = 2\mathcal{X}^{\mathrm{T}}\mathcal{P}\dot{\mathcal{X}} \quad \text{such that} -\gamma_1 \leq C^{\mathrm{T}}\mathcal{X} \leq \gamma_2. \tag{4.2}$$

By substituting the expression from Eq (3.11) into (4.2), we can express it as follows:

$$\dot{\mathcal{V}}(\mathcal{X}) = 2\mathcal{X}^{\mathrm{T}}\mathcal{P}(\mathcal{A}+\mathcal{B}\mathcal{K})\mathcal{X} + 2\mathcal{X}^{\mathrm{T}}\mathcal{P}\mathcal{B}u_{nl} + 2\mathcal{X}^{\mathrm{T}}\mathcal{P}\mathcal{D}_1\Phi_1(\mathcal{X}) + 2\mathcal{X}^{\mathrm{T}}\mathcal{P}\mathcal{D}_2\Phi_3(\mathcal{X}) + 2\mathcal{X}^{\mathrm{T}}\mathcal{P}\mathcal{B}\Delta_t. \quad (4.3)$$

To improve the control effectiveness and guarantee exponential stability, we introduce the following criterion:

$$\dot{\mathcal{V}}(\mathcal{X}) + \eta\mathcal{V}(\mathcal{X}) < 0, \quad (4.4)$$

where $\eta > 0$ is a positive scalar.

For the stability of the controlled robot, we will utilize the expression developed in (4.3). This leads to the formulation of two distinct LMI conditions for the gain matrix $\mathcal{K}$, which will be elaborated upon in the following sections.

4.1. First LMI-based design strategy

In this first approach, we aim to stabilize the knee exoskeleton robot by considering a bounded form of the nonlinear term $\Phi_3(\mathcal{X})$ [18]. Starting from the expanded Lyapunov function derivative in (4.3), we systematically develop an LMI condition to compute the gain matrix $\mathcal{K}$.

First, recall that $\Phi_1(\mathcal{X}) = \mathrm{sgn}(\dot{\phi}) = \pm 1$, which directly implies $\Phi_1(\mathcal{X})^2 = 1$. Applying Young's inequality [19] to the cross-term that involves $\Phi_1(\mathcal{X})$, we obtain the following:

$$2\mathcal{X}^{\mathrm{T}}\mathcal{P}\mathcal{D}_1\Phi_1(\mathcal{X}) \leq \mathcal{X}^{\mathrm{T}}\mathcal{P}\mathcal{M}_1\mathcal{P}\mathcal{X} + \mathcal{D}_1^{\mathrm{T}}\mathcal{M}_1^{-1}\mathcal{D}_1, \quad (4.5)$$

where $\mathcal{M}_1 = \mathcal{M}_1^{\mathrm{T}} > 0$ is a positive definite matrix.

Next, for the term that involves $\Phi_3(\mathcal{X})$, which is a scalar function defined in (3.12), Young's inequality similarly yields the following:

$$2\mathcal{X}^{\mathrm{T}}\mathcal{P}\mathcal{D}_2\Phi_3(\mathcal{X}) \leq \mathcal{X}^{\mathrm{T}}\mathcal{P}\mathcal{M}_2\mathcal{P}\mathcal{X} + \mathcal{D}_2^{\mathrm{T}}\mathcal{M}_2^{-1}\mathcal{D}_2\Phi_3(\mathcal{X})^2, \quad (4.6)$$

where $\mathcal{M}_2 = \mathcal{M}_2^{\mathrm{T}} > 0$.

To further handle $\Phi_3(\mathcal{X})^2$, note that, for angles $0^\circ \leq \theta \leq 90^\circ$, the following inequalities hold:

$$\cos^2(\theta) \leq 1, \quad (4.7a)$$

$$-2\cos(\theta) \leq 0. \quad (4.7b)$$

Expanding $\Phi_3(\mathcal{X})^2$ from (3.12) leads to the following:

$$\Phi_3(\mathcal{X})^2 = \cos^2(\theta) - 2\cos(\theta_d)\cos(\theta) + \cos^2(\theta_d). \quad (4.8)$$

Applying inequalities (4.7), we conclude the following:

$$\Phi_3(\mathcal{X})^2 \leq \mu_{11}, \quad (4.9)$$

where $\mu_{11} = 1 + \cos^2(\theta_d) > 0$.

Consequently, Expression (4.6) can be reformulated as follows:

$$2\mathcal{X}^{\mathrm{T}}\mathcal{P}\mathcal{D}_2\Phi_3(\mathcal{X}) \leq \mathcal{X}^{\mathrm{T}}\mathcal{P}\mathcal{M}_2\mathcal{P}\mathcal{X} + \mu_{11}\mathcal{D}_2^{\mathrm{T}}\mathcal{M}_2^{-1}\mathcal{D}_2. \quad (4.10)$$

Similarly, to manage the disturbance term $2\mathcal{X}^{\mathrm{T}}\mathcal{P}\mathcal{B}\Delta_t$, we normalize Δ_t with its known upper bound $\bar{\delta}$ and apply Young's inequality as follows:

$$2\mathcal{X}^{\mathrm{T}}\mathcal{P}\mathcal{B}\Delta_t \leq m_3\bar{\delta}^2\mathcal{X}^{\mathrm{T}}\mathcal{P}\mathcal{B}\mathcal{B}^{\mathrm{T}}\mathcal{P}\mathcal{X} + m_3^{-1}\left(\frac{\Delta_t}{\bar{\delta}}\right)^2, \quad (4.11)$$

where $m_3 = m_3^{\mathrm{T}} > 0$.

By assuming $\left\|\frac{\Delta_t}{\bar{\delta}}\right\| \leq 1$, we deduce the following:

$$\left(\frac{\Delta_t}{\bar{\delta}}\right)^2 \leq 1. \quad (4.12)$$

Therefore, the following inequality can be established:

$$2\mathcal{X}^{\mathrm{T}}\mathcal{P}\mathcal{B}\Delta_t \leq m_3\bar{\delta}^2\mathcal{X}^{\mathrm{T}}\mathcal{P}\mathcal{B}\mathcal{B}^{\mathrm{T}}\mathcal{P}\mathcal{X} + m_3^{-1}. \quad (4.13)$$

By inserting Eqs (4.5), (4.10), and (4.13) into Expression (4.3) and considering (4.4), the derivative of the Lyapunov function satisfies the following:

$$\begin{aligned}\dot{\mathcal{V}}(\mathcal{X}) + \eta\mathcal{V}(\mathcal{X}) = \mathcal{X}^{\mathrm{T}}\Big((\mathcal{P}\mathcal{A}+\mathcal{P}\mathcal{B}\mathcal{K}) + (\mathcal{P}\mathcal{A}+\mathcal{P}\mathcal{B}\mathcal{K})^{\mathrm{T}} \\ +\mathcal{P}\mathcal{M}_1\mathcal{P} + \mathcal{P}\mathcal{M}_2\mathcal{P} + m_3\bar{\delta}^2\mathcal{P}\mathcal{B}\mathcal{B}^{\mathrm{T}}\mathcal{P} + \eta\mathcal{P}\Big)\mathcal{X} \\ + 2\mathcal{X}^{\mathrm{T}}\mathcal{P}\mathcal{B}u_{nl} + \mathcal{D}_1^{\mathrm{T}}\mathcal{M}_1^{-1}\mathcal{D}_1 + \mu_{11}\mathcal{D}_2^{\mathrm{T}}\mathcal{M}_2^{-1}\mathcal{D}_2 + m_3^{-1}.\end{aligned} \quad (4.14)$$

We define the auxiliary nonlinear controller u_{nl} in the following manner:

$$u_{nl} = \begin{cases} -\frac{1}{2}\frac{\mathcal{B}^{\mathrm{T}}\mathcal{P}\mathcal{X}}{\mathcal{X}^{\mathrm{T}}\mathcal{P}\mathcal{B}\mathcal{B}^{\mathrm{T}}\mathcal{P}\mathcal{X}}\lambda & \text{if} \quad \|\mathcal{B}^{\mathrm{T}}\mathcal{P}\mathcal{X}\|^2 > \kappa \\ -\frac{1}{2}\frac{\mathcal{B}^{\mathrm{T}}\mathcal{P}\mathcal{X}}{\kappa}\lambda & \text{if} \quad \|\mathcal{B}^{\mathrm{T}}\mathcal{P}\mathcal{X}\|^2 \leq \kappa \end{cases} \quad (4.15)$$

where $\kappa > 0$ is a positive scalar.

In addition, the scalar function λ is introduced as:

$$\lambda = \mathcal{D}_1^{\mathrm{T}}\mathcal{M}_1^{-1}\mathcal{D}_1 + \mu_{11}\mathcal{D}_2^{\mathrm{T}}\mathcal{M}_2^{-1}\mathcal{D}_2 + m_3^{-1}. \quad (4.16)$$

When the condition $||\mathcal{B}^{\mathrm{T}}\mathcal{P}\mathcal{X}||^2 > \kappa$ holds, substituting the control law u_{nl} from (4.15) into inequality (4.14) simplifies it to the following:

$$\begin{aligned}\dot{\mathcal{V}}(\mathcal{X}) + \eta\mathcal{V}(\mathcal{X}) \leq \mathcal{X}^{\mathrm{T}}\Big((\mathcal{P}\mathcal{A} + \mathcal{P}\mathcal{B}\mathcal{K}) + (\mathcal{P}\mathcal{A} + \mathcal{P}\mathcal{B}\mathcal{K})^{\mathrm{T}} \\ +\mathcal{P}\mathcal{M}_1\mathcal{P} + \mathcal{P}\mathcal{M}_2\mathcal{P} + m_3\bar{\delta}^2\mathcal{P}\mathcal{B}\mathcal{B}^{\mathrm{T}}\mathcal{P} + \eta\mathcal{P}\Big)\mathcal{X}. \quad (4.17)\end{aligned}$$

In contrast, if we consider the scenario where $||\mathcal{B}^{\mathrm{T}}\mathcal{P}\mathcal{X}||^2 \leq \kappa$, we again utilize the definition of u_{nl} from Eq (4.15). This substitution transforms inequality (4.14) into the following expression:

$$\begin{aligned}\dot{\mathcal{V}}(\mathcal{X}) + \eta\mathcal{V}(\mathcal{X}) \leq \mathcal{X}^{\mathrm{T}}\Big((\mathcal{P}\mathcal{A} + \mathcal{P}\mathcal{B}\mathcal{K}) + (\mathcal{P}\mathcal{A} + \mathcal{P}\mathcal{B}\mathcal{K})^{\mathrm{T}} \\ +\mathcal{P}\mathcal{M}_1\mathcal{P} + \mathcal{P}\mathcal{M}_2\mathcal{P} + m_3\bar{\delta}^2\mathcal{P}\mathcal{B}\mathcal{B}^{\mathrm{T}}\mathcal{P} + \eta\mathcal{P}\Big)\mathcal{X} \\ + \lambda\left(1 - \frac{||\mathcal{B}^{\mathrm{T}}\mathcal{P}\mathcal{X}||^2}{\kappa}\right). \quad (4.18)\end{aligned}$$

Given that $\frac{||\mathcal{B}^{\mathrm{T}}\mathcal{P}\mathcal{X}||^2}{\kappa} \leq 1$ and that $\lambda > 0$, we can derive the following conclusion:

$$\lambda\left(1 - \frac{||\mathcal{B}^{\mathrm{T}}\mathcal{P}\mathcal{X}||^2}{\kappa}\right) \geq 0. \quad (4.19)$$

From this analysis, the Lyapunov function $\mathcal{V}(\mathcal{X})$, as defined in Eq (4.1), is obviously constrained under these conditions. Consequently, when $||\mathcal{B}^{\mathrm{T}}\mathcal{P}\mathcal{X}||^2 \leq \kappa$, the closed-loop system's trajectory remains restricted. Therefore, the critical task reduces to verifying the stability condition presented in inequality (4.17).

To establish the LMI conditions, we begin by defining the function $\mathcal{Z}(\mathcal{X})$ as follows:

$$\begin{aligned}\mathcal{Z}(\mathcal{X}) =& 2\mathcal{X}^{\mathrm{T}}\mathcal{P}(\mathcal{A} + \mathcal{B}\mathcal{K})\mathcal{X} + \mathcal{X}^{\mathrm{T}}\mathcal{P}\mathcal{M}_1\mathcal{P}\mathcal{X} + \mathcal{X}^{\mathrm{T}}\mathcal{P}\mathcal{M}_2\mathcal{P}\mathcal{X} \\ &+ m_3\bar{\delta}^2\mathcal{X}^{\mathrm{T}}\mathcal{P}\mathcal{B}\mathcal{B}^{\mathrm{T}}\mathcal{P}\mathcal{X} + \eta\mathcal{X}^{\mathrm{T}}\mathcal{P}\mathcal{X}. \quad (4.20)\end{aligned}$$

This expression can be rewritten as follows:

$$\mathcal{Z}(\mathcal{X}) = \begin{bmatrix} \mathcal{X} \\ 1 \end{bmatrix}^{\mathrm{T}} \begin{bmatrix} \Upsilon_{11} & \mathcal{O} \\ \star & \mathcal{O} \end{bmatrix} \begin{bmatrix} \mathcal{X} \\ 1 \end{bmatrix} < 0, \quad (4.21)$$

with $\Upsilon_{11} = (\mathcal{P}\mathcal{A} + \mathcal{P}\mathcal{B}\mathcal{K}) + (\mathcal{P}\mathcal{A} + \mathcal{P}\mathcal{B}\mathcal{K})^{\mathrm{T}} + \mathcal{P}\mathcal{M}_1\mathcal{P} + \mathcal{P}\mathcal{M}_2\mathcal{P} + m_3\bar{\delta}^2\mathcal{P}\mathcal{B}\mathcal{B}^{\mathrm{T}}\mathcal{P} + \eta\mathcal{P}$.

In this context, the notation $\star$ indicates the term obtained by transposing the corresponding element, while $\mathcal{I}$ and $\mathcal{O}$ denote the identity matrix and the zero matrix, respectively, with suitable sizes.

The conditions which pertain to the nonlinear controller u_{nl}, as introduced in Eq (4.15), can be rewritten as follows:

$$\begin{bmatrix} \mathcal{X} \\ 1 \end{bmatrix}^{\mathrm{T}} \begin{bmatrix} \mathcal{P}\mathcal{B}\mathcal{B}^{\mathrm{T}}\mathcal{P} & \mathcal{O} \\ \star & -\kappa \end{bmatrix} \begin{bmatrix} \mathcal{X} \\ 1 \end{bmatrix} \geq 0. \quad (4.22)$$

Furthermore, the constraints associated with the defined Lyapunov function $\mathcal{V}(\mathcal{X})$, as described in (4.1), are reformulated as follows:

$$\begin{bmatrix} \mathcal{X} \\ 1 \end{bmatrix}^{\mathrm{T}} \begin{bmatrix} \mathcal{O} & \mathcal{C} \\ \star & -2\gamma_2 \end{bmatrix} \begin{bmatrix} \mathcal{X} \\ 1 \end{bmatrix} \leq 0, \quad (4.23)$$

$$\begin{bmatrix} \mathcal{X} \\ 1 \end{bmatrix}^{\mathrm{T}} \begin{bmatrix} \mathcal{O} & -\mathcal{C} \\ \star & -2\gamma_1 \end{bmatrix} \begin{bmatrix} \mathcal{X} \\ 1 \end{bmatrix} \leq 0. \quad (4.24)$$

Utilizing the S-procedure, as discussed in [19], and considering Eqs (4.21)–(4.24), we arrive at the following condition:

$$\begin{bmatrix} \Upsilon_{11} + \beta_3\mathcal{P}\mathcal{B}\mathcal{B}^{\mathrm{T}}\mathcal{P} & -(\beta_1 - \beta_2)\mathcal{C} \\ \star & 2\gamma_2\beta_1 + 2\gamma_1\beta_2 - \kappa\beta_3 \end{bmatrix} < 0, \quad (4.25)$$

where $\beta_1 > 0, \beta_2 > 0$, and $\beta_3 > 0$.

Therefore, we will multiply the obtained condition (4.25) from both sides by $Q = \mathrm{diag}(\mathcal{S}, \mathcal{I})$, where $\mathcal{S} = \mathcal{P}^{-1}$, thus yielding the following:

$$\begin{bmatrix} \Sigma_{11} & -(\beta_1 - \beta_2)\mathcal{S}\mathcal{C} \\ \star & \Sigma_{22} \end{bmatrix} < 0, \quad (4.26)$$

where

$$\begin{aligned}\Sigma_{11} =& (\mathcal{A}\mathcal{S} + \mathcal{B}\mathcal{R}) + (\mathcal{A}\mathcal{S} + \mathcal{B}\mathcal{R})^{\mathrm{T}} + \mathcal{M}_1 + \mathcal{M}_2 + m_3\bar{\delta}^2\mathcal{B}\mathcal{B}^{\mathrm{T}} \\ &+ \eta\mathcal{S} + \beta_3\mathcal{B}\mathcal{B}^{\mathrm{T}}, \quad (4.27a) \\ \Sigma_{22} =& 2\gamma_2\beta_1 + 2\gamma_1\beta_2 - \kappa\beta_3, \quad (4.27b)\end{aligned}$$

with $\mathcal{R} = \mathcal{K}\mathcal{S}$.

For the sake of clarity, we introduce the following definitions: $\xi^{-1} = -\kappa\beta_3$, $\sigma_1 = \beta_1^{-1}$, $\sigma_2 = \beta_2^{-1}$, $\mathcal{G} = \begin{bmatrix} -\mathcal{S}\mathcal{C} & \mathcal{S}\mathcal{C} \end{bmatrix}$, $\mathcal{L} = \begin{bmatrix} \mathcal{I} \\ \mathcal{I} \end{bmatrix}$, $\mathcal{N} = \begin{bmatrix} \sigma_1 & \mathcal{O} \\ \mathcal{O} & \sigma_2 \end{bmatrix}$, and $Q^{-1} = \begin{bmatrix} 2\gamma_2 & \mathcal{O} \\ \mathcal{O} & 2\gamma_1 \end{bmatrix}$. Additionally, we pose the following:

$$\begin{aligned}\Lambda = (\mathcal{A}\mathcal{S} + \mathcal{B}\mathcal{R}) + (\mathcal{A}\mathcal{S} + \mathcal{B}\mathcal{R})^{\mathrm{T}} + \mathcal{M}_1 + \mathcal{M}_2 \\ + m_3\bar{\delta}^2\mathcal{B}\mathcal{B}^{\mathrm{T}} + \beta_3\mathcal{B}\mathcal{B}^{\mathrm{T}} + \eta\mathcal{S}. \quad (4.28)\end{aligned}$$

Under these new notations, the matrix inequality given in (4.26) can be equivalently expressed as follows:

$$\begin{bmatrix} \Lambda & \mathcal{G}\mathcal{N}^{-1}\mathcal{L} \\ \star & \mathcal{L}^{\mathrm{T}}(\mathcal{Q}\mathcal{N})^{-1}\mathcal{L}+\xi^{-1} \end{bmatrix} < 0. \tag{4.29}$$

By using the Schur complement lemma in conjunction with the matrix inequality in (4.29), we can derive the subsequent conditions:

$$\mathcal{L}^{\mathrm{T}}(\mathcal{Q}\mathcal{N})^{-1}\mathcal{L}+\xi^{-1} < 0, \tag{4.30}$$

$$\Lambda - \left(\mathcal{G}\mathcal{N}^{-1}\mathcal{L}\right)\left(\mathcal{L}^{\mathrm{T}}(\mathcal{Q}\mathcal{N})^{-1}\mathcal{L}+\xi^{-1}\right)^{-1}\left(\mathcal{G}\mathcal{N}^{-1}\mathcal{L}\right)^{\mathrm{T}} < 0. \tag{4.31}$$

To simplify the inversion that appears in (4.31), we apply the matrix inversion lemma [19], which leads to the following:

$$\left(\mathcal{L}^{\mathrm{T}}(\mathcal{Q}\mathcal{N})^{-1}\mathcal{L}+\xi^{-1}\right)^{-1} = \xi - \xi^2\mathcal{L}^{\mathrm{T}}\mathcal{H}^{-1}\mathcal{L}, \tag{4.32}$$

where

$$\mathcal{H} = \xi\mathcal{L}\mathcal{L}^{\mathrm{T}} + \mathcal{Q}\mathcal{N}. \tag{4.33}$$

Substituting (4.32) into (4.31) leads to the following:

$$\Lambda - \left(\mathcal{G}\mathcal{N}^{-1}\mathcal{L}\right)\left(\xi - \xi^2\mathcal{L}^{\mathrm{T}}\mathcal{H}^{-1}\mathcal{L}\right)\left(\mathcal{G}\mathcal{N}^{-1}\mathcal{L}\right)^{\mathrm{T}} < 0. \tag{4.34}$$

We define the following:

$$\Pi = \left(\mathcal{G}\mathcal{N}^{-1}\mathcal{L}\right)\left(\xi - \xi^2\mathcal{L}^{\mathrm{T}}\mathcal{H}^{-1}\mathcal{L}\right)\left(\mathcal{G}\mathcal{N}^{-1}\mathcal{L}\right)^{\mathrm{T}}. \tag{4.35}$$

Expanding the expression in Eq (4.35), given that both $\mathcal{N}$ and $\mathcal{H}$ are symmetric, we obtain the following:

$$\Pi = \xi\mathcal{G}\mathcal{N}^{-1}\mathcal{L}\mathcal{L}^{\mathrm{T}}\mathcal{N}^{-1}\mathcal{G}^{\mathrm{T}} - \xi^2\mathcal{G}\mathcal{N}^{-1}\mathcal{L}\mathcal{L}^{\mathrm{T}}\mathcal{H}^{-1}\mathcal{L}\mathcal{L}^{\mathrm{T}}\mathcal{N}^{-1}\mathcal{G}^{\mathrm{T}}. \tag{4.36}$$

Using the expression of $\mathcal{H}$, we can simplify each term as follows:

$$\xi\mathcal{G}\mathcal{N}^{-1}\mathcal{L}\mathcal{L}^{\mathrm{T}}\mathcal{N}^{-1}\mathcal{G}^{\mathrm{T}} = \mathcal{G}\mathcal{N}^{-1}\mathcal{H}\mathcal{N}^{-1}\mathcal{G}^{\mathrm{T}} - \mathcal{G}\mathcal{N}^{-1}\mathcal{Q}\mathcal{G}^{\mathrm{T}}, \tag{4.37a}$$

$$\xi^2\mathcal{G}\mathcal{N}^{-1}\mathcal{L}\mathcal{L}^{\mathrm{T}}\mathcal{H}^{-1}\mathcal{L}\mathcal{L}^{\mathrm{T}}\mathcal{N}^{-1}\mathcal{G}^{\mathrm{T}} = \mathcal{G}\mathcal{N}^{-1}\mathcal{H}\mathcal{N}^{-1}\mathcal{G}^{\mathrm{T}} - 2\mathcal{G}\mathcal{Q}\mathcal{N}^{-1}\mathcal{G}^{\mathrm{T}} + \mathcal{G}\mathcal{Q}\mathcal{H}^{-1}\mathcal{Q}\mathcal{G}^{\mathrm{T}}. \tag{4.37b}$$

By combining (4.37a) and (4.37b), we obtain the following compact expression for Π:

$$\Pi = \mathcal{G}\mathcal{Q}\mathcal{N}^{-1}\mathcal{G}^{\mathrm{T}} - \mathcal{G}\mathcal{Q}\mathcal{H}^{-1}\mathcal{Q}\mathcal{G}^{\mathrm{T}}. \tag{4.38}$$

Therefore, by substituting the preceding expression in (4.38) into Eq (4.34), we derive the following:

$$\Lambda - \mathcal{G}\mathcal{Q}\mathcal{N}^{-1}\mathcal{G}^{\mathrm{T}} + \mathcal{G}\mathcal{Q}\mathcal{H}^{-1}\mathcal{Q}\mathcal{G}^{\mathrm{T}} < 0. \tag{4.39}$$

For clarity, we define the following terms:

$$\mathcal{G}\mathcal{Q}\mathcal{N}^{-1}\mathcal{G}^{\mathrm{T}} = \frac{1}{2\gamma_2}\beta_1\mathcal{S}CC^{\mathrm{T}}\mathcal{S} + \frac{1}{2\gamma_1}\beta_2\mathcal{S}CC^{\mathrm{T}}\mathcal{S}. \tag{4.40a}$$

Consequently, using these expressions, we can easily demonstrate the following inequality:

$$\Lambda - \frac{1}{2\gamma_2}\beta_1\mathcal{S}CC^{\mathrm{T}}\mathcal{S} - \frac{1}{2\gamma_1}\beta_2\mathcal{S}CC^{\mathrm{T}}\mathcal{S} + \mathcal{G}\mathcal{Q}\mathcal{H}^{-1}\mathcal{Q}\mathcal{G}^{\mathrm{T}} < 0. \tag{4.41}$$

Considering the augmented matrix $\bar{C} = \begin{bmatrix} 1 & 0 \\ 0 & 0 \end{bmatrix}$, we can show the following:

$$-\frac{1}{2\gamma_2}\beta_1\mathcal{S}CC^{\mathrm{T}}\mathcal{S} = \rho_1^{-1}\beta_1\mathcal{S}\bar{C}\bar{C}^{\mathrm{T}}\mathcal{S}, \tag{4.42a}$$

$$-\frac{1}{2\gamma_1}\beta_2\mathcal{S}CC^{\mathrm{T}}\mathcal{S} = \rho_2^{-1}\beta_2\mathcal{S}\bar{C}\bar{C}^{\mathrm{T}}\mathcal{S}, \tag{4.42b}$$

where $\rho_1^{-1} = -\frac{1}{2\gamma_2}$, and $\rho_2^{-1} = -\frac{1}{2\gamma_1}$.

Thus, utilizing (4.42), we can rewrite inequality (4.41) as follows:

$$\Lambda + \rho_1^{-1}\beta_1\mathcal{S}\bar{C}\bar{C}^{\mathrm{T}}\mathcal{S} + \rho_2^{-1}\beta_2\mathcal{S}\bar{C}\bar{C}^{\mathrm{T}}\mathcal{S} + \mathcal{G}\mathcal{Q}\mathcal{H}^{-1}\mathcal{Q}\mathcal{G}^{\mathrm{T}} < 0. \tag{4.43}$$

Given that $\rho_1^{-1} < 0$ and $\beta_1 > 0$, it follows that $\rho_1^{-1}\beta_1\mathcal{S}\bar{C}\bar{C}^{\mathrm{T}}\mathcal{S} < 0$. By applying Young's inequality, we can bound it as follows:

$$\rho_1^{-1}\beta_1\mathcal{S}\bar{C}\bar{C}^{\mathrm{T}}\mathcal{S} \leq -\rho_1\sigma_1\mathcal{I} - \mathcal{S}\bar{C} - \bar{C}^{\mathrm{T}}\mathcal{S}. \tag{4.44}$$

Similarly, since $\rho_2^{-1} < 0$ and $\beta_2 > 0$, we have the following:

$$\rho_2^{-1}\beta_2\mathcal{S}\bar{C}\bar{C}^{\mathrm{T}}\mathcal{S} \leq -\rho_2\sigma_2\mathcal{I} - \mathcal{S}\bar{C} - \bar{C}^{\mathrm{T}}\mathcal{S}. \tag{4.45}$$

By substituting (4.44) and (4.45) into Eq (4.43), we can express it as follows:

$$\Lambda - \rho_1\sigma_1\mathcal{I} - \rho_2\sigma_2\mathcal{I} - 2\mathcal{S}\bar{\mathcal{C}} - 2\bar{\mathcal{C}}^{\mathrm{T}}\mathcal{S} + \mathcal{G}\mathcal{Q}\mathcal{H}^{-1}\mathcal{Q}\mathcal{G}^{\mathrm{T}} < 0. \tag{4.46}$$

Furthermore, under the assumptions that $\xi < 0$, $\mathcal{L}\mathcal{L}^{\mathrm{T}} > 0$, and $\mathcal{N} > 0$, it follows that $\mathcal{H} > 0$. Consequently, by applying the Schur complement to inequality (4.46), we obtain the following equivalent condition:

$$\begin{bmatrix} \Lambda - \rho_1\sigma_1\mathcal{I} - \rho_2\sigma_2\mathcal{I} - 2\mathcal{S}\bar{\mathcal{C}} - 2\bar{\mathcal{C}}^{\mathrm{T}}\mathcal{S} & \mathcal{G}\mathcal{Q} \\ \star & -\mathcal{H} \end{bmatrix} < 0. \tag{4.47}$$

By setting $\alpha_1 = m_3^{-1}$ and $\alpha_2 = \frac{1}{\beta_3\kappa}$ and appropriately redefining Λ, $\mathcal{G}$, $\mathcal{Q}$, and $\mathcal{H}$ in (4.47), we can reformulate the above inequality as the following LMI:

$$\begin{bmatrix} \Xi_{11} & -\frac{1}{2\gamma_2}\mathcal{S}\mathcal{C} & \frac{1}{2\gamma_1}\mathcal{S}\mathcal{C} & \bar{\delta}\mathcal{B} \\ \star & \alpha_2\mathcal{I} - \frac{1}{2\gamma_2}\sigma_1 & \alpha_2\mathcal{I} & \mathcal{O} \\ \star & \star & \alpha_2\mathcal{I} - \frac{1}{2\gamma_1}\sigma_2 & \mathcal{O} \\ \star & \star & \star & -\alpha_1\mathcal{I} \end{bmatrix} < 0, \tag{4.48}$$

where $\Xi_{11} = (\mathcal{A}\mathcal{S} + \mathcal{B}\mathcal{R}) + (\mathcal{A}\mathcal{S} + \mathcal{B}\mathcal{R})^{\mathrm{T}} + \mathcal{M}_1 + \mathcal{M}_2 + \beta_3\mathcal{B}\mathcal{B}^{\mathrm{T}} + \eta\mathcal{S} - \rho_1\sigma_1\mathcal{I} - \rho_2\sigma_2\mathcal{I} - 2\mathcal{S}\bar{\mathcal{C}} - 2\bar{\mathcal{C}}^{\mathrm{T}}\mathcal{S}$.

In addition, by using Eq (4.30) and multiplying it by ξ^2, we derive the following inequality:

$$\xi^2\mathcal{L}^{\mathrm{T}}(\mathcal{Q}\mathcal{N})^{-1}\mathcal{L} + \xi < 0. \tag{4.49}$$

Given that $\mathcal{Q}\mathcal{N} > 0$ and $\xi < 0$, we can apply the Schur complement to (4.49) to obtain the following equivalent LMI:

$$\begin{bmatrix} \xi & \xi\mathcal{L}^{\mathrm{T}} \\ \star & -\mathcal{Q}\mathcal{N} \end{bmatrix} < 0. \tag{4.50}$$

We derive the following second LMI:

$$\begin{bmatrix} -\alpha_2\mathcal{I} & -\alpha_2\mathcal{I} & -\alpha_2\mathcal{I} \\ \star & -\frac{1}{2\gamma_2}\sigma_1 & \mathcal{O} \\ \star & \star & -\frac{1}{2\gamma_1}\sigma_2 \end{bmatrix} < 0. \tag{4.51}$$

It is crucial to emphasize that the stability criteria presented in (4.48) and (4.51) correspond to an LMI expressed through the unknown variables $\mathcal{S}$, $\mathcal{R}$, $\mathcal{M}_1$, $\mathcal{M}_2$, β_3, α_1, α_2, σ_1, σ_2, and $\bar{\delta}$.

Theorem 4.1. *Let us consider positive definite matrices $\mathcal{S}$, $\mathcal{M}_1$, and $\mathcal{M}_2$, and a matrix $\mathcal{R}$, along with scalar variables β_3, α_1, α_2, σ_1, σ_2, and $\bar{\delta}$, that satisfy the following LMI condition for a fixed scalar $\eta \geq 0$:*

$$\begin{bmatrix} \left\{ \begin{array}{c} (\mathcal{A}\mathcal{S} + \mathcal{B}\mathcal{R}) + (\mathcal{A}\mathcal{S} + \mathcal{B}\mathcal{R})^{\mathrm{T}} \\ +\mathcal{M}_1 + \mathcal{M}_2 + \beta_3\mathcal{B}\mathcal{B}^{\mathrm{T}} - \rho_1\sigma_1\mathcal{I} \\ -\rho_2\sigma_2\mathcal{I} - 2\mathcal{S}\bar{\mathcal{C}} - 2\bar{\mathcal{C}}^{\mathrm{T}}\mathcal{S} + \eta\mathcal{S} \end{array} \right\} & -\frac{1}{2\gamma_2}\mathcal{S}\mathcal{C} & \frac{1}{2\gamma_1}\mathcal{S}\mathcal{C} & \bar{\delta}\mathcal{B} \\ \star & \alpha_2\mathcal{I} - \frac{1}{2\gamma_2}\sigma_1 & \alpha_2\mathcal{I} & \mathcal{O} \\ \star & \star & \alpha_2\mathcal{I} - \frac{1}{2\gamma_1}\sigma_2 & \mathcal{O} \\ \star & \star & \star & -\alpha_1\mathcal{I} \end{bmatrix} < 0, \tag{4.52a}$$

$$\begin{bmatrix} -\alpha_2\mathcal{I} & -\alpha_2\mathcal{I} & -\alpha_2\mathcal{I} \\ \star & -\frac{1}{2\gamma_2}\sigma_1 & \mathcal{O} \\ \star & \star & -\frac{1}{2\gamma_1}\sigma_2 \end{bmatrix} < 0. \tag{4.52b}$$

Then, the dynamic model of the knee-joint exoskeleton system, as described by (2.4), will be stabilized by the control law presented in (3.8). Furthermore, the feedback gain $\mathcal{K}$ of the adopted controller can be computed using the following expression:

$$\mathcal{K} = \mathcal{R}\mathcal{S}^{-1}. \tag{4.53}$$

4.2. Second LMI-based design strategy

In this section, we propose a second method to formulate the LMI conditions for the computation of the feedback gain matrix $\mathcal{K}$. Specifically, we consider the case where the nonlinear function $\Phi_3(\mathcal{X})$ is constrained by a linear expression [18,31]. Following the same structure as in (4.3), we aim to derive alternative LMI criteria.

First, it is important to observe that $\Phi_1(\mathcal{X}) = \mathrm{sgn}(\dot{\phi}) = \pm 1$. Consequently, we have $\Phi_1(\mathcal{X})^2 = 1$, which directly leads to the simplifications used in (4.5).

Next, treating $\Phi_3(\mathcal{X})$ as a scalar function according to (3.12), we apply Young's inequality to the term $2\mathcal{X}^{\mathrm{T}}\mathcal{P}\mathcal{D}_2\Phi_3(\mathcal{X})$ in (4.3), thus yielding the following:

$$2\mathcal{X}^{\mathrm{T}}\mathcal{P}\mathcal{D}_2\Phi_3(\mathcal{X}) \leq m_2\mathcal{X}^{\mathrm{T}}\mathcal{P}\mathcal{D}_2\mathcal{D}_2^{\mathrm{T}}\mathcal{P}\mathcal{X} + m_2^{-1}\Phi_3(\mathcal{X})^2, \tag{4.54}$$

where $m_2 > 0$.

Utilizing the expression from (3.6), leads to the following:

$$\Phi_3(\mathcal{X})^2 = \cos^2(\theta) + \cos^2(\theta_d) - 2\cos(\theta_d)\cos(\theta). \quad (4.55)$$

Then, we use the following bounds:

$$\cos^2(\theta) \leq 1, \quad (4.56a)$$

$$-2\cos(\theta) \leq a_2\theta + b_2, \quad (4.56b)$$

with constants $a_2 = \frac{4}{\pi}$ and $b_2 = -2$.

From this, we derive an upper bound for the cross term as follows:

$$-2\cos(\theta)\cos(\theta_d) \leq a_2\theta_d\cos(\theta_d) + a_2\cos(\theta_d)\phi + b_2\cos(\theta_d). \quad (4.57)$$

Thus, $\Phi_3(\mathcal{X})^2$ is bounded as follows:

$$\Phi_3(\mathcal{X})^2 \leq 2\mu_{21}\phi + \mu_{22}, \quad (4.58)$$

where μ_{21} and μ_{22} are defined by the following quantities:

$$\mu_{21} = \frac{a_2}{2}\cos(\theta_d) > 0, \quad (4.59a)$$

$$\mu_{22} = 1 + a_2\cos(\theta_d)\theta_d + b_2\cos(\theta_d) + \cos^2(\theta_d). \quad (4.59b)$$

Assuming that the variable ϕ is linearly related to the state vector by $\phi = C_1\mathcal{X}$, with $C_1 = \begin{bmatrix} 1 & 0 \end{bmatrix}$, we can reformulate Eq (4.58) as follows:

$$\Phi_3(\mathcal{X})^2 \leq 2\mu_{21}C_1\mathcal{X} + \mu_{22}. \quad (4.60)$$

Substituting this into (4.54) leads to the following:

$$2\mathcal{X}^{\mathrm{T}}\mathcal{P}\mathcal{D}_2\Phi_3(\mathcal{X}) \leq m_2\mathcal{X}^{\mathrm{T}}\mathcal{P}\mathcal{D}_2\mathcal{D}_2^{\mathrm{T}}\mathcal{P}\mathcal{X} + 2\mu_{21}m_2^{-1}C_1\mathcal{X} + \mu_{22}m_2^{-1}. \quad (4.61)$$

Moreover, by treating Δ_t as a scalar function, we can invoke the Young inequality lemma on the term $2\mathcal{X}^{\mathrm{T}}\mathcal{P}\mathcal{B}\Delta_t$ in Eq (4.3). Assuming that Δ_t meets the constraint established in (4.12), we can subsequently derive the inequalities presented in (4.13).

By substituting Eqs (4.5), (4.13), and (4.61) into inequality (4.3) and integrating the constraint from (4.4), we arrive at the subsequent inequality:

$$\begin{aligned}\dot{\mathcal{V}}(\mathcal{X}) + \eta\mathcal{V}(\mathcal{X}) = \mathcal{X}^{\mathrm{T}}\Big(&(\mathcal{P}\mathcal{A} + \mathcal{P}\mathcal{B}\mathcal{K}) + (\mathcal{P}\mathcal{A} + \mathcal{P}\mathcal{B}\mathcal{K})^{\mathrm{T}} \\ &+\mathcal{P}\mathcal{M}_1\mathcal{P} + m_2\mathcal{P}\mathcal{D}_2\mathcal{D}_2^{\mathrm{T}}\mathcal{P} + m_3\bar{\delta}^2\mathcal{P}\mathcal{B}\mathcal{B}^{\mathrm{T}}\mathcal{P} + \eta\mathcal{P}\Big)\mathcal{X} \\ &+ 2\mathcal{X}^{\mathrm{T}}\mathcal{P}\mathcal{B}u_{nl} + \mathcal{D}_1^{\mathrm{T}}\mathcal{M}_1^{-1}\mathcal{D}_1 + 2\mu_{21}m_2^{-1}C_1\mathcal{X} \\ &+ \mu_{22}m_2^{-1} + m_3^{-1}.\end{aligned} \quad (4.62)$$

The same auxiliary nonlinear controller u_{nl}, which is specified in Eq (4.15), is also taken into consideration.

Then, we define the following specific formulation for the function λ:

$$\lambda = \mathcal{D}_1^{\mathrm{T}}\mathcal{M}_1^{-1}\mathcal{D}_1 + 2\mu_{21}m_2^{-1}C_1\mathcal{X} + \mu_{22}m_2^{-1} + m_3^{-1}. \quad (4.63)$$

Remark 4.1. *Various expressions for the function λ have been proposed in the literature. For instance, in our previous works, λ was defined as follows:*

$$\lambda = \mathcal{D}_1^{\mathrm{T}}\mathcal{M}_1^{-1}\mathcal{D}_1 + \mu_1\mathcal{D}_2^{\mathrm{T}}\mathcal{M}_2^{-1}\mathcal{D}_2 + \bar{\delta}^2\mathcal{B}^{\mathrm{T}}\mathcal{M}_3^{-1}\mathcal{B}. \quad (4.64)$$

Modifying the definition of the parameter λ allows the development of distinct control strategies, thus offering flexibility in tuning the controller to improve its adaptability and performance under varying conditions.

In this study, we use two distinct expressions for the parameter λ, presented in Eqs (4.16) and (4.63), to address different design requirements. Each approximation of the nonlinear term $\Phi_3(\mathcal{X})$ allows us to develop a specific and appropriate expression for λ. For instance, by approximating the nonlinear term $\Phi_3(\mathcal{X})$ using a constant constraint (4.9), we define the corresponding expression for λ given by (4.16). Similarly, by approximating the nonlinear term $\Phi_3(\mathcal{X})$ with a first-order linear constraint (4.60), we define the suitable expression for λ given by (4.63). Thus, for each approximation, it is necessary to define a specific expression for λ in order to develop a robust control strategy that captures the system dynamics and disturbances, thus enhancing robustness against significant external influences.

When the condition $\|\mathcal{B}^{\mathrm{T}}\mathcal{P}\mathcal{X}\|^2 > \kappa$ is met, substituting the expression for u_{nl} in (4.62), we can simplify it to the following:

$$\dot{\mathcal{V}}(\mathcal{X}) + \eta\mathcal{V}(\mathcal{X}) \le \mathcal{X}^{\mathrm{T}}\Big((\mathcal{P}\mathcal{A} + \mathcal{P}\mathcal{B}\mathcal{K}) + (\mathcal{P}\mathcal{A} + \mathcal{P}\mathcal{B}\mathcal{K})^{\mathrm{T}} + \mathcal{P}\mathcal{M}_1\mathcal{P} + m_2\mathcal{P}\mathcal{D}_2\mathcal{D}_2^{\mathrm{T}}\mathcal{P} + m_3\bar{\delta}^2\mathcal{P}\mathcal{B}\mathcal{B}^{\mathrm{T}}\mathcal{P} + \eta\mathcal{P}\Big)\mathcal{X}. \tag{4.65}$$

Conversely, when the condition $\|\mathcal{B}^{\mathrm{T}}\mathcal{P}\mathcal{X}\|^2 \le \kappa$ is satisfied, inequality (4.62) can be restructured as follows:

$$\begin{aligned}\dot{\mathcal{V}}(\mathcal{X}) + \eta\mathcal{V}(\mathcal{X}) \le{}& \mathcal{X}^{\mathrm{T}}\Big((\mathcal{P}\mathcal{A} + \mathcal{P}\mathcal{B}\mathcal{K}) + (\mathcal{P}\mathcal{A} + \mathcal{P}\mathcal{B}\mathcal{K})^{\mathrm{T}} \\ &+ \mathcal{P}\mathcal{M}_1\mathcal{P} + m_2\mathcal{P}\mathcal{D}_2\mathcal{D}_2^{\mathrm{T}}\mathcal{P} + m_3\bar{\delta}^2\mathcal{P}\mathcal{B}\mathcal{B}^{\mathrm{T}}\mathcal{P} + \eta\mathcal{P}\Big)\mathcal{X} \\ &+ \lambda\left(1 - \frac{\|\mathcal{B}^{\mathrm{T}}\mathcal{P}\mathcal{X}\|^2}{\kappa}\right).\end{aligned} \tag{4.66}$$

Given that $\frac{\|\mathcal{B}^{\mathrm{T}}\mathcal{P}\mathcal{X}\|^2}{\kappa} \le 1$ and $\lambda > 0$, the function $\mathcal{V}(\mathcal{X})$ remains constrained, thus ensuring that the closed-loop system's trajectory remains stable under the condition $\|\mathcal{B}^{\mathrm{T}}\mathcal{P}\mathcal{X}\|^2 \le \kappa$. Now, the task is to validate the condition outlined in (4.65).

It is important to highlight that the structure of (4.65) closely resembles that of (4.17). Therefore, by employing similar analytical techniques and setting $\alpha_1 = m_3^{-1}$ and $\alpha_2 = \frac{1}{\beta_3\kappa}$, we can establish the following LMI-based stability conditions:

$$\begin{bmatrix} \Xi_{22} & -\frac{1}{2\gamma_2}\mathcal{S}\mathcal{C} & \frac{1}{2\gamma_1}\mathcal{S}\mathcal{C} & \bar{\delta}\mathcal{B} \\ \star & \alpha_2\mathcal{I} - \frac{1}{2\gamma_2}\sigma_1 & \alpha_2\mathcal{I} & \mathcal{O} \\ \star & \star & \alpha_2\mathcal{I} - \frac{1}{2\gamma_1}\sigma_2 & \mathcal{O} \\ \star & \star & \star & -\alpha_1\mathcal{I} \end{bmatrix} < 0, \tag{4.67}$$

$$\begin{bmatrix} -\alpha_2\mathcal{I} & -\alpha_2\mathcal{I} & -\alpha_2\mathcal{I} \\ \star & -\frac{1}{2\gamma_2}\sigma_1 & \mathcal{O} \\ \star & \star & -\frac{1}{2\gamma_1}\sigma_2 \end{bmatrix} < 0, \tag{4.68}$$

where $\Xi_{22} = (\mathcal{A}\mathcal{S} + \mathcal{B}\mathcal{R}) + (\mathcal{A}\mathcal{S} + \mathcal{B}\mathcal{R})^{\mathrm{T}} + \mathcal{M}_1 + \tau_2\mathcal{D}_2\mathcal{D}_2^{\mathrm{T}} + \beta_3\mathcal{B}\mathcal{B}^{\mathrm{T}} + \eta\mathcal{S} - \rho_1\sigma_1\mathcal{I} - \rho_2\sigma_2\mathcal{I} - 2\mathcal{S}\bar{\mathcal{C}} - 2\bar{\mathcal{C}}^{\mathrm{T}}\mathcal{S}$

We have established the LMI conditions, specifically (4.67) and (4.68), characterized by the unknown matrix variables $\mathcal{S}$, $\mathcal{R}$, and $\mathcal{M}_1$, in addition to the unknown scalar variables β_3, α_1, α_2, σ_1, σ_2, m_2, and $\bar{\delta}$.

Theorem 4.2. *Assuming the presence of positive definite symmetric matrices $\mathcal{S}$ and $\mathcal{M}_1$, along with matrix $\mathcal{R}$, and scalar variables β_3, α_1, α_2, σ_1, σ_2, m_2, and $\bar{\delta}$, the following conditions, for a fixed scalar $\eta \ge 0$, are satisfied:*

$$\begin{bmatrix} \left\{\begin{array}{c} (\mathcal{A}\mathcal{S} + \mathcal{B}\mathcal{R}) + (\mathcal{A}\mathcal{S} + \mathcal{B}\mathcal{R})^{\mathrm{T}} \\ +\mathcal{M}_1 + \tau_2\mathcal{D}_2\mathcal{D}_2^{\mathrm{T}} + \beta_3\mathcal{B}\mathcal{B}^{\mathrm{T}} \\ -\rho_1\sigma_1\mathcal{I} - \rho_2\sigma_2\mathcal{I} \\ -2\mathcal{S}\bar{\mathcal{C}} - 2\bar{\mathcal{C}}^{\mathrm{T}}\mathcal{S} + \eta\mathcal{S} \end{array}\right\} & -\frac{1}{2\gamma_2}\mathcal{S}\mathcal{C} & \frac{1}{2\gamma_1}\mathcal{S}\mathcal{C} & \bar{\delta}\mathcal{B} \\ \star & \alpha_2\mathcal{I} - \frac{1}{2\gamma_2}\sigma_1 & \alpha_2\mathcal{I} & \mathcal{O} \\ \star & \star & \alpha_2\mathcal{I} - \frac{1}{2\gamma_1}\sigma_2 & \mathcal{O} \\ \star & \star & \star & -\alpha_1\mathcal{I} \end{bmatrix} < 0, \tag{4.69a}$$

$$\begin{bmatrix} -\alpha_2\mathcal{I} & -\alpha_2\mathcal{I} & -\alpha_2\mathcal{I} \\ \star & -\frac{1}{2\gamma_2}\sigma_1 & \mathcal{O} \\ \star & \star & -\frac{1}{2\gamma_1}\sigma_2 \end{bmatrix} < 0; \tag{4.69b}$$

therefore, the control approach outlined in (3.8), (3.9), and (4.15) will effectively stabilize the dynamic behavior of the knee exoskeleton system (2.4). Moreover, the feedback gain $\mathcal{K}$ of the adopted controller can be computed using Expression (4.53).

Remark 4.2. *In the first design method, we approximate the nonlinear term $\Phi_3(\mathcal{X})$ using a constant constraint (4.9). This simplification keeps the constraints manageable while ensuring stability in the exoskeleton's position control. For the second design method, we apply a first-order linear constraint for $\Phi_3(\mathcal{X})$, which is more conservative as it introduces terms that involve θ_d and ϕ (see Eq (4.60)). This allows an improved handling of nonlinearities, though it is more conservative than the constant constraint. Although higher-order or nonlinear constraints could be used, we chose the first-order linear approach to balance the modeling accuracy with computational simplicity. This method provides more tractable stability conditions within the LMI-based design framework, while effectively capturing the key nonlinear dynamics that affect the system's behavior.*

Remark 4.3. *LMI techniques have emerged as a cornerstone in modern control system design due to their flexibility, robustness, and ability to simultaneously address multiple performance objectives [34, 35]. By* *formulating control problems as convex optimization problems, LMI methods provide powerful and systematic tools to handle dynamic feedback stabilization, robust performance, gain-scheduling, and regional pole placement. In the field of rehabilitation robotics, particularly for lower-limb exoskeletons, LMIs have been successfully applied to manage the challenges associated with nonlinear dynamics, human-robot interaction, and uncertainty [36–38]. Their adaptability ensures stability and robustness across different patient profiles and dynamic scenarios. Moreover, the integration of LMIs with fuzzy control and adaptive strategies has further enhanced their ability to address complex, real-world conditions in assistive robotic devices [39, 40]. Supported by efficient computational tools, such as MATLAB's LMI toolbox, and solid theoretical foundations such as the Lyapunov stability theory, LMI-based control design offers a reliable, scalable, and high-performance framework. Given these strengths, the proposed controller benefits from the inherent advantages of LMI formulations, thus making it particularly well-suited for the robust and adaptive control of knee rehabilitation exoskeletons.*

5. Simulation outcomes

This section discusses the outcomes of the two control techniques applied in this work. The primary aim is to validate that the derived LMI criteria are effective in determining the gain $\mathcal{K}$ of the controller, which ensures the stabilization of the knee-joint exoskeleton, as depicted in Figure 1. Table 1 presents a detailed list of the robot's specific parameters, which are determined by the dynamic Eq (2.4).

Table 1. Selected parameters values for the knee exoskeleton robot.

Parameter	Value	Nominal parameter	Nominal value	Unit
ϑ	0.323 + 0.1	$\vartheta_\star$	0.323	Kg.m^2/rad
m	0.1 + 0.01	$m_\star$	0.1	Kg
l	0.25 + 0.05	$l_\star$	0.25	m
f_v	0.35 + 0.1	$f_v^\star$	0.35	N.m.s/rad
f_s	0.059 + 0.05	$f_s^\star$	0.059	N.m/A
g	9.8			

It is crucial to emphasize that our attention is centered on presenting numerical simulation results for the diverse control methods utilized in this study. A subsequent comparative analysis between these methods will be undertaken.

We set the desired position to $\theta_d = 30°$. Furthermore, a random signal Δ_t is introduced as an external disturbance, only active between 2 and 7 seconds, and is set to zero outside of this interval. The disturbance Δ_t is defined by the following expression:

$$\Delta_t = \bar{\delta} \times (2 \times \text{rand} - 1), \tag{5.1}$$

where rand generates a random value in the range $\begin{bmatrix} 0 & 1 \end{bmatrix}$.

5.1. Outcomes from the first design method

By applying the LMI conditions outlined in Theorem 4.1, we solve the LMI-based problem with $\alpha = 5$. This yields the following results:

$$\mathcal{K} = \begin{bmatrix} -44.3161 - 11.6947 \end{bmatrix}, \tag{5.2a}$$

$$\kappa = 0.2305, \tag{5.2b}$$

$$\bar{\delta} = 2.1178. \tag{5.2c}$$

By incorporating the feedback gain $\mathcal{K}$ from (5.2) into the controller (3.8), we obtain the simulation outcomes presented in Figure 2. The figures show that the robot successfully achieves the desired state. Additionally, the control input u approaches u_d at the equilibrium point.

5.2. Outcomes from the second design method

Using the second design methodology based on the LMI conditions from Theorem 4.2, we solve the associated LMI problem and select $\alpha = 6$. The resulting values are as follows:

$$\mathcal{K} = \begin{bmatrix} -69.9283 & -15.0494 \end{bmatrix}, \tag{5.3a}$$

$$\kappa = 0.1622, \tag{5.3b}$$

$$\bar{\delta} = 2.7377. \tag{5.3c}$$

By implementing the feedback gain $\mathcal{K}$ from (5.3) into the control law (3.8), the simulation results are represented in Figure 3. These results confirm that the exoskeleton robot reaches the desired position, with the control input u approaching u_d as the system stabilizes.

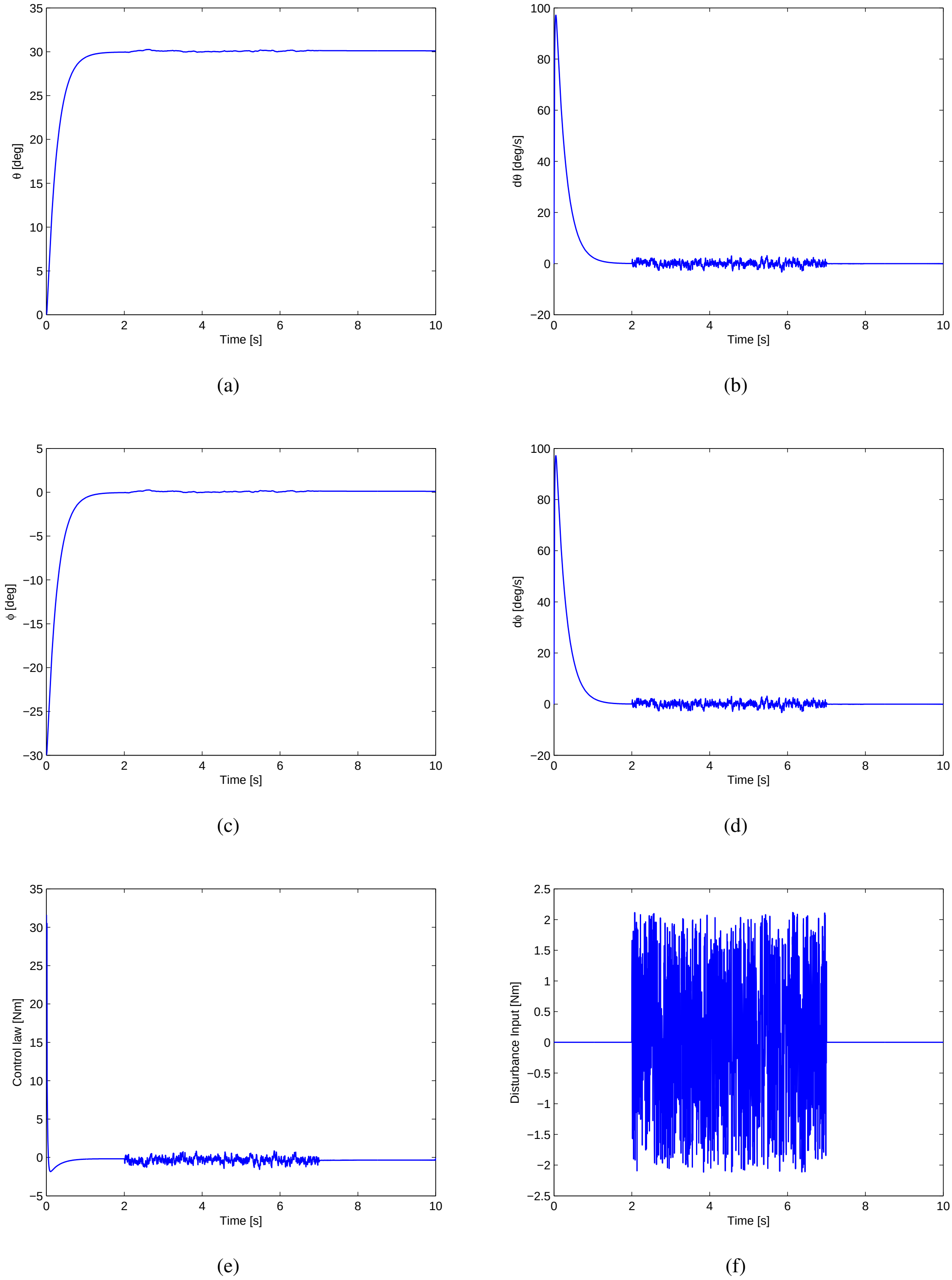

Figure 2. Simulation outcomes utilizing the first control approach. Evolution of the following: (a) angular position θ, (b) angular velocity $\dot{\theta}$, (c) angular position error ϕ, (d) angular velocity error $\dot{\phi}$, (e) nonlinear composite controller u, and (f) external disturbance Δ_t.

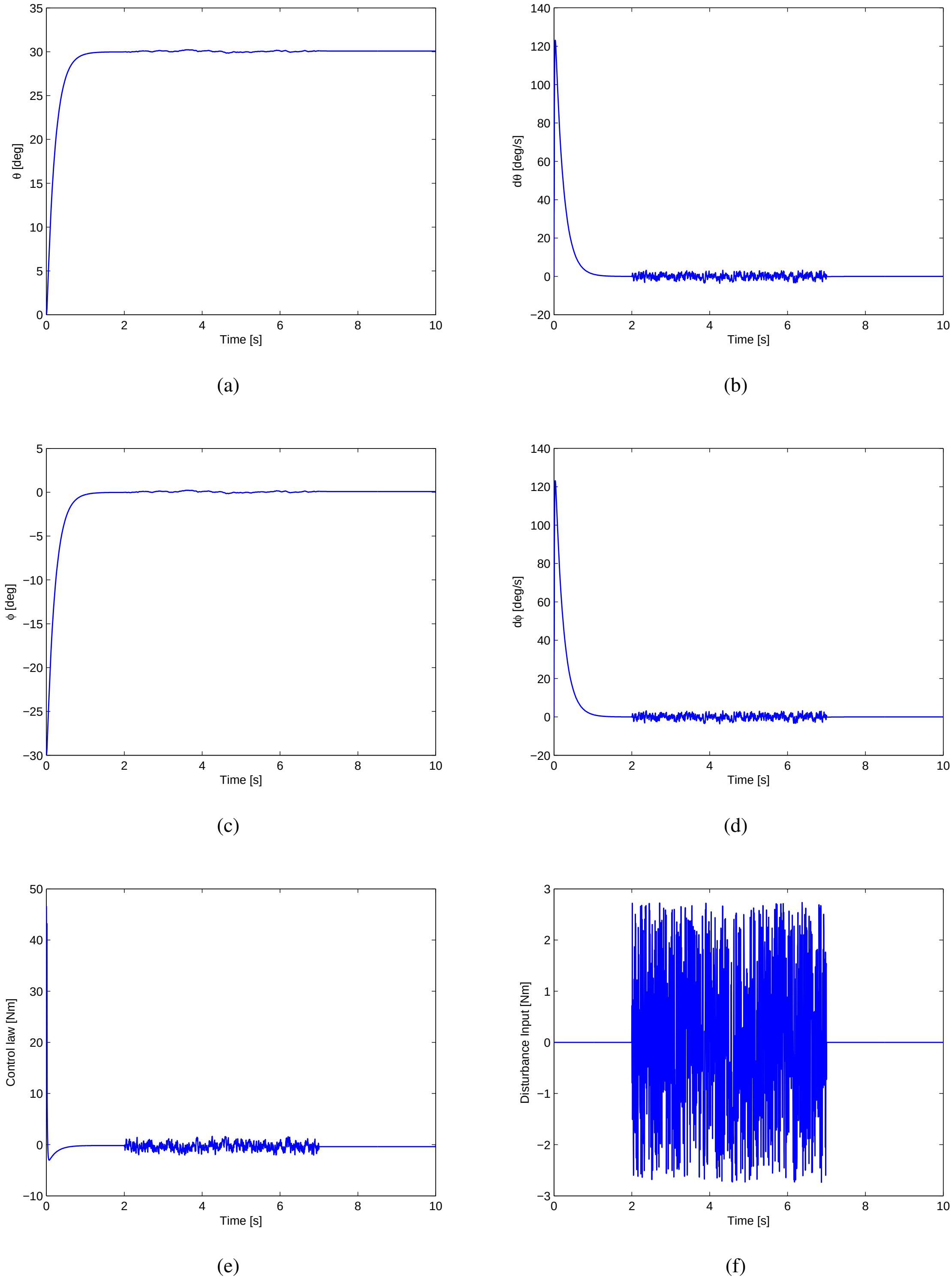

Figure 3. Simulation outcomes utilizing the second control approach. Evolution of the following: (a) angular position θ, (b) angular velocity $\dot{\theta}$, (c) angular position error ϕ, (d) angular velocity error $\dot{\phi}$, (e) nonlinear composite controller u, and (f) external disturbance Δ_t.

In addition to the simulation results, we investigated the temporal evolution of the variable λ, as shown in Figure 4 (see Eq (4.63)). The fluctuations in λ highlight the controller's dynamic adjustments aimed at ensuring the system stability. As the exoskeleton moves towards its target position, λ stabilizes, thus reflecting the system's convergence to the desired state.

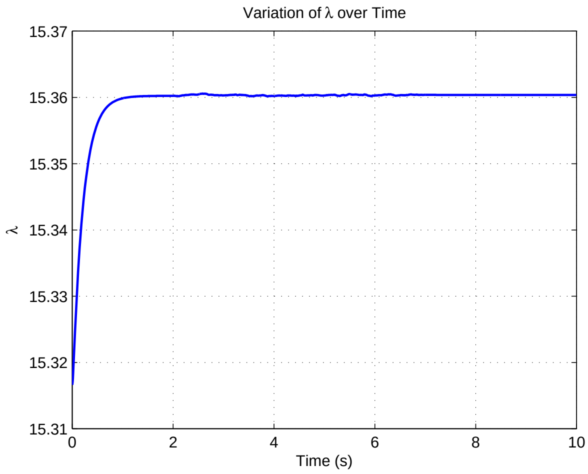

Figure 4. Time variation of the function λ defined by Expression (4.63) using the second design approach.

Remark 5.1. *Notice that, in the previous theorems, Theorems 4.1 and 4.2, the LMI-based problems formulated already provide a feedback gain $\mathcal{K}$ of the proposed control law with an acceptable magnitude ((5.2) and (5.3), respectively). As a result, there was no need to introduce additional conditions to limit the size of the controller gain [19]. Such constraints would only be necessary if the computed feedback gains were excessively large, which would make it impractical for real-world implementation. Since the gain derived from the current formulation is within reasonable bounds, these additional conditions are not required in this context.*

5.3. Discussion

The controller proposed in this study successfully regulates the position of the knee-joint exoskeleton robotic system, as demonstrated by Figure 1. This is achieved by employing two different methodologies to calculate the feedback gain, thereby allowing the robotic system to consistently reach the intended state θ_d. Clearly, from Figures 2(a) and 3(a), the angular position θ approaches the desired value. Similarly, Figures 2(b) and 3(b) show that the angular velocities $\dot{\theta}$ converge to zero. As a result, the angular position error ϕ ultimately becomes zero, as depicted in Figures 2(c) and 3(c), and the angular velocity error $\dot{\phi}$ also tends towards zero, as shown in Figures 2(d) and 3(d). Although slight oscillations are observed due to the applied disturbance torque Δ_t, the results confirm the robustness of the controller in reducing the effects of external disturbances.

The external disturbances applied to the knee exoskeleton are visually represented in Figure 2(f) and 3(f), with the disturbance characterized by the torque load Δ_t. This disturbance is modeled as a random signal, varying within the range of $-\bar{\delta}$ to $\bar{\delta}$, and is only active between 2 and 7 seconds. The effect of this disturbance is seen in Figures 2 and 3, where the system exhibits oscillations around its equilibrium state. As the disturbance diminishes, the controlled knee exoskeleton returns to its target position. The disturbance amplitude obtained using the first design method is $\bar{\delta} = 2.1178$, while the second method yields an amplitude of $\bar{\delta} = 2.7377$.

Furthermore, the time evolution of the applied control law u is illustrated in Figures 2(e) and 3(e). These figures show that as the knee-joint exoskeleton stabilizes under the impact of the external torque, the control input u approaches the target control u_d.

Notice that the control effort u applied to the joint in both methodologies remains within acceptable limits, as depicted in Figures 2(e) and 3(e). However, the first design method consistently results in a lower initial control effort compared to the second design method. Specifically, in the first simulation using the initial approach, at the beginning of the simulation, the control effort is 31.62 (as shown in Figure 2(e)), while the second approach yields a control effort of 46.63 at the beginning of the simulation (depicted in Figure 3(e)).

In addition, it is important to highlight that the values of κ and $\bar{\delta}$ are nearly the same across both methodologies, as indicated in (5.2) and (5.3). Notably, the results from the second design method show a slightly lower value for κ

compared to the first design method. Conversely, the second design method yields a slightly higher value for $\bar{\delta}$ than that obtained using the first design method. Therefore, the results from both design methodologies demonstrate the successful regulation of the knee-joint exoskeleton, thus effectively reaching the desired state. As a result, the controller for the knee exoskeleton robot is validated as effective.

Additionally, the inclusion of state constraints (3.1) enhances the system stability, reduces an unnecessary control effort, and ensures that the controller operates within the physical limits of the knee joint. Consequently, the effectiveness of the composite controller was evaluated using various metrics across the two design methodologies, as detailed in Table 2. The Mean Absolute Error (MAE) for the joint angle (ϕ) was recorded at 0.0152 for the first approach and 0.0125 for the second approach. Similarly, the MAE for joint velocity ($\dot{\phi}$) was recorded at 0.0603 for the first approach and 0.0618 for the second approach. Regarding the Mean Squared Error (MSE), the values for the joint angle (ϕ) were 0.0040 and 0.0033 for approaches 1 and 2, respectively. For the joint velocity ($\dot{\phi}$), the MSE recorded was 0.0509 for approach 1 and 0.0629 for approach 2. The Root Mean Squared Error (RMSE) exhibited a comparable pattern, with recorded values of 0.0635 and 0.0573 for the joint angle (ϕ) for approaches 1 and 2, respectively. For the joint velocity ($\dot{\phi}$), the RMSE was 0.2256 and 0.2508 for approaches 1 and 2, respectively. These findings highlight the controller's effectiveness in delivering accurate and resilient control for knee exoskeleton systems.

Table 2. Evaluation of the proposed composite controller's performance through different design methodologies utilizing a range of performance metrics/indicators.

Indicator	Approach 1	Approach 2
MAE (ϕ)	0.0152	0.0125
MAE $(\dot{\phi})$	0.0603	0.0618
MSE (ϕ)	0.0040	0.0033
MSE $(\dot{\phi})$	0.0509	0.0629
RMSE (ϕ)	0.0635	0.0573
RMSE $(\dot{\phi})$	0.2256	0.2508

To further evaluate the robustness of the proposed LMI-based composite controller, a parameter sensitivity analysis was conducted. As detailed in Table 1, key physical parameters of the knee exoskeleton robot, including the inertia ϑ, mass m, link length l, viscous friction coefficient f_v, and static friction coefficient f_s, were intentionally varied from their nominal values. These variations simulate realistic uncertainties that may occur due to modeling errors or system wear. The simulation results demonstrated that, even with these parameter deviations, the controller maintained a stable performance and accurate position control. Specifically, the increases in the MAE and RMSE remained marginal, thus indicating a minimal degradation of control accuracy. Furthermore, the stability of the closed-loop system was preserved without any signs of oscillations or instability. This confirms the strong robustness of the proposed approach against parameter uncertainties, thus making it highly suitable for practical rehabilitation applications where the system parameters are rarely perfectly known.

Based on the overall simulation results and performance analysis, it can be concluded that the two design methodologies offer complementary strengths and weaknesses, thus enabling a tailored selection according to application priorities. The first design methodology is characterized by a significantly lower initial control effort, with a value of 31.62 compared to 46.63 for the second method. This feature makes it particularly suitable for applications where minimizing the actuator wear and energy consumption is a primary concern. Moreover, it results in slightly lower oscillations under external disturbances, as indicated by a lower disturbance amplitude ($\bar{\delta}$ = 2.1178). Although its tracking performance is slightly less accurate than that of the second method, with higher MAE and RMSE values for the joint angle ϕ, the difference remains minor and acceptable for most rehabilitation tasks.

Conversely, the second design methodology prioritizes the tracking accuracy, thereby achieving lower MAE and RMSE values for the joint angle ϕ (MAE = 0.0125, RMSE = 0.0573). This makes it particularly appropriate for applications where precise joint positioning is critical, such as fine rehabilitation exercises or tasks that require strict motion control. However, this improved accuracy comes at the cost of a higher initial control effort and a slightly greater disturbance amplitude ($\bar{\delta} = 2.7377$), thus indicating a somewhat increased sensitivity to external perturbations.

5.4. Comparison with classical controllers

Moreover, to reinforce the validation of the proposed LMI-based composite controller, a comprehensive qualitative and quantitative comparison was conducted with well-established control strategies, namely classical PD, PID, and affine state-feedback controllers. While these conventional methods are widely adopted due to their simplicity and ease of implementation, they suffer from significant limitations when confronted with strong nonlinearities, external disturbances, and parameter uncertainties. For example, Munadi et al. [41] demonstrated that PID controllers perform reasonably well in mildly nonlinear systems but fail to maintain stability and precision under more complex and dynamic conditions. Similarly, Touati et al. [42] reported notable challenges in applying PID control for lower-limb rehabilitation when dynamic disturbances were present. Even advanced variants such as the adaptive PID controllers proposed by Liu et al. [21], which incorporate optimization techniques such as PSO, exhibit a high sensitivity to parameter variations and model mismatches.

In contrast, the proposed composite controller leverages a robust mathematical framework based on LMIs, which allows for the systematic incorporation of nonlinearities, model uncertainties, and external disturbances into the control design. To ensure a fair and consistent evaluation, we adopt the same test conditions as those used in [19]. Specifically, the desired angular position is set to $\theta_d = 40°$, and the external disturbance is modeled as $\Delta_t = \bar{\delta} \times \sin(\omega_f \times t)$, where ω_f is the frequency of the sinusoidal disturbance, chosen here as $\omega_f = 5\pi$. This setup guarantees a valid basis for direct performance comparison.

The comparative study, summarized in Table 3, evaluates three key performance metrics: the feedback gain vector ($\mathcal{K}^{\mathrm{T}}$), the maximum admissible disturbance torque ($\bar{\delta}$), and the stabilization time (t_s). The results clearly demonstrate the superior performance of the proposed composite controller, particularly in terms of the disturbance rejection and the stabilization speed. Both design approaches of the composite controller (Approaches 1 and 2) outperform the affine and PID controllers in terms of robustness to external perturbations and the ability to achieve faster convergence. Notably, Approach 2 achieves the shortest stabilization time of 1.3 seconds and the highest disturbance rejection capability with $\bar{\delta} = 2.7$, thus highlighting its strong potential for use in dynamic and uncertain rehabilitation environments. The selection between the two methodologies should be based on the specific objectives of the application. When minimizing the control effort and reducing the mechanical stress on the system are the main concerns, the first design methodology is preferable. Conversely, when achieving the highest possible position accuracy is the priority, the second design methodology is recommended, even if it requires a higher control energy. This improvement illustrates the flexibility of the proposed method in balancing performance and robustness according to application needs. Overall, the findings confirm that the proposed LMI-based control strategy provides a more resilient and accurate solution than traditional control approaches, especially when operating in nonlinear and uncertain conditions commonly encountered in rehabilitation scenarios.

Table 3. Performance metrics for the composite, affine state-feedback, and PID controller: feedback fain, disturbance rejection, and stabilization time.

Metric	Composite Controller (App 1)	Composite Controller (App 2)	Controller	PID Controller
$\mathcal{K}^{\mathrm{T}}$	$\begin{bmatrix} -44.10 \\ -11.83 \end{bmatrix}$	$\begin{bmatrix} -68.11 \\ -14.93 \end{bmatrix}$	$\begin{bmatrix} -3.24 \\ -1.20 \end{bmatrix}$	$\begin{bmatrix} -6.89 \\ -1.62 \\ -7.22 \end{bmatrix}$
$\bar{\delta}$	2.1	2.7	0.84	0.81
t_s [s]	1.7	1.3	1.4	2.5

6. Conclusions and future works

This study presented a robust control strategy specifically designed for a 1-DoF knee rehabilitation exoskeleton robot, thereby emphasizing accurate position control to tackle issues such as state constraints, parameter uncertainties, and external disturbances. We employed two distinct design methodologies to derive the LMI stability criteria for the gain of the proposed composite control law. Our methodology leverages a quadratic

Lyapunov candidate and integrates various mathematical techniques, including the Schur complement, Young's inequality, the S-procedure lemma and the matrix inversion lemma. The formulated LMIs guarantee robust stability of the knee-joint exoskeleton despite uncertainties and external influences. To validate the proposed control strategy, extensive simulation studies were conducted. The quantitative performance evaluation demonstrated that the first design methodology significantly reduced the initial control effort (31.62 compared to 46.63 for the second method) and achieved better disturbance rejection (disturbance amplitude $\bar{\delta} = 2.1178$ versus $\bar{\delta} = 2.7377$). Meanwhile, the second methodology achieved a superior tracking accuracy, with lower MAE and RMSE values for the joint angle ϕ (MAE = 0.0125, RMSE = 0.0573), compared to the first method (MAE = 0.0152, RMSE = 0.0635). These numerical results highlight a clear trade-off between minimizing the control energy and maximizing the tracking precision, thus offering practical guidance to select the appropriate design methodology based on specific rehabilitation objectives. Overall, the proposed controller proved effective in delivering reliable, accurate, and robust position control for knee rehabilitation exoskeletons, thus contributing valuable insights to the advancement of wearable robotic rehabilitation systems.

Looking ahead, future work will focus on several key directions. First, we plan to implement a filtering mechanism to reduce the amplitude and duration of oscillations observed in the controlled system. Additionally, we intend to conduct comprehensive experimental tests to validate the proposed LMI-based control framework, thereby assessing its robustness under various practical conditions and addressing challenges such as actuator saturation. Additionally, future research will explore the integration of nonlinear control laws for both position regulation and motion (trajectory tracking) control of the knee exoskeleton robot. Another important direction will be the development of static or dynamic output feedback controllers, particularly in scenarios where direct measurements of the knee joint velocity are not available. Furthermore, we plan to extend this study by conducting a comparative analysis with standard robust control strategies, such as H_2 and H_∞ controllers, to further assess the advantages and limitations of our method in practical rehabilitation scenarios.

Use of Generative-AI tools declaration

The authors declare they have not used Artificial Intelligence (AI) tools in the creation of this article.

Conflict of interest

The authors declare there is no conflict of interest.

References

1. M. Jakovljevic, R. Westerman, T. Sharma, D. Lamnisos, Aging and global health, In: R. Haring, I. Kickbusch, D. Ganten, M. Moeti, *Handbook of global health*, Springer, Cham, 2020, 73–102. https://doi.org/10.1007/978-3-030-05325-3_4-1
2. S. Sunde, K. Hesseberg, D. A. Skelton, A. H. Ranhoff, A. H. Pripp, M. Aarønæs, et al., Associations between health-related quality of life and physical function in older adults with or at risk of mobility disability after discharge from the hospital, *Eur. Geriatr. Med.*, **12** (2021), 1247–1256. https://doi.org/10.1007/s41999-021-00525-0
3. O. Boubaker, *Medical and healthcare robotics: new paradigms and recent advances*, 1 Ed., Elsevier, Academic Press, 2023. https://doi.org/10.1016/C2022-0-00158-6
4. P. K. Lingampally, K. C. Ramanathan, R. Shanmugam, L. Cepova, S. Salunkhe, Wearable assistive rehabilitation robotic devices—a comprehensive review, *Machines*, **12** (2024), 415. https://doi.org/10.3390/machines12060415
5. T. N. Bryce, V. Huang, M. X. Escalon, Spinal cord injury, In: D. X. Cifu, *Braddom's physical medicine and rehabilitation*, 6 Eds., Philadelphia: Elsevier, 2021. https://doi.org/10.1016/B978-0-323-62539-5.00049-7

6. A. Garcia-Gonzalez, R. Q. Fuentes-Aguilar, I. Salgado, I. Chairez, A review on the application of autonomous and intelligent robotic devices in medical rehabilitation, *J. Braz. Soc. Mech. Sci. Eng.*, **44** (2022), 393. https://doi.org/10.1007/s40430-022-03692-8

7. R. S. Baragash, H. Aldowah, S. Ghazal, Virtual and augmented reality applications to improve older adults' quality of life: a systematic mapping review and future directions, *Digit. Health*, **8** (2022), 1–34. https://doi.org/10.1177/20552076221132099

8. S. Arof, E. Noorsal, S. Z. Yahaya, Z. Hussain, Y. Mohd Ali, M. H. Abdullah, et al., Adaptive sliding mode feedback control algorithm for a nonlinear knee extension model, *Machines*, **11** (2023), 732. https://doi.org/10.3390/machines11070732

9. M. Khamar, M. Edrisi, Designing a backstepping sliding mode controller for an assistant human knee exoskeleton based on nonlinear disturbance observer, *Mechatronics*, **54** (2018), 121–132. https://doi.org/10.1016/j.mechatronics.2018.07.010

10. G. Mashud, S. K. Hasan, N. Alam, Advances in control techniques for rehabilitation exoskeleton robots: a systematic review, *Actuators*, **14** (2025), 108. https://doi.org/10.3390/act14030108

11. M. E. Daachi, T. Madani, B. Daachi, K. Djouani, A radial basis function neural network adaptive controller to drive a powered lower limb knee joint orthosis, *Appl. Soft Comput.*, **34** (2015), 324–336. https://doi.org/10.1016/j.asoc.2015.04.034

12. T. Madani, B. Daachi, K. Djouani, Non-singular terminal sliding mode controller: application to an actuated exoskeleton, *Mechatronics*, **33** (2016), 136–145. https://doi.org/10.1016/j.mechatronics.2015.10.012

13. J. Wang, J. Liu, L. Chen, S. Guo, Observer-based finite-time control for trajectory tracking of lower extremity exoskeleton, *Proc. Inst. Mech. Eng., Part I: J. Syst. Control Eng.*, **236** (2022), 257–269. https://doi.org/10.1177/09596518211033728

14. N. A. Alawad, A. J. Humaidi, A. S. Alaraji, Sliding mode-based active disturbance rejection control of assistive exoskeleton device for rehabilitation of disabled lower limbs, *An. Acad. Bras. Ciênc.,* **95** (2023), e20220680. https://doi.org/10.1590/0001-3765202320220680

15. A. Q. Al-Dujaili, A. F. Hasan, A. J. Humaidi, A. Al-Jodah, Anti-disturbance control design of exoskeleton knee robotic system for rehabilitative care, *Heliyon*, **10** (2024), e28911. https://doi.org/10.1016/j.heliyon.2024.e28911

16. N. A. Alawad, A. J. Humaidi, A. S. Alaraji, Design of active disturbance rejection control for rehabilitation-assistant device of lower limbs under cross coupling effect, *Proc. Inst. Mech. Eng. Part C J. Mech. Eng. Sci.*, **238** (2024), 7388–7398. https://doi.org/10.1177/09544062241232230

17. N. A. Alawad, A. J. Humaidi, A. S. Al-Araji, Error-based ADRC approach of lower knee exoskeleton system for rehabilitation, *Int. J. Autom. Control*, **19** (2025), 1–17. https://doi.org/10.1504/IJAAC.2025.142972

18. S. Jenhani, H. Gritli, An LMI-based robust state-feedback controller design for the position control of a knee rehabilitation exoskeleton robot: comparative analysis, *Meas. Control*, **57** (2024), 1326–1346. https://doi.org/10.1177/00202940241236295

19. S. Jenhani, H. Gritli, J. Narayan, Robust position control of a knee-joint rehabilitation exoskeleton using a linear matrix inequalities-based design approach, *Appl. Sci.*, **15** (2025), 404. https://doi.org/10.3390/app15010404

20. K. I. Sherwani, N. Kumar, A. Chemori, M. Khan, S. Mohammed, Rise-based adaptive control for eicosi exoskeleton to assist knee joint mobility, *Robot. Auton. Syst.*, **124** (2020), 103354. https://doi.org/10.1016/j.robot.2019.103354

21. J. Liu, H. Fang, J. Xu, Online adaptive PID control for a multi-joint lower extremity exoskeleton system using improved particle swarm optimization, *Machines*, **10** (2022), 21. https://doi.org/10.3390/machines10010021

22. A. S. Aljuboury, A. H. Hameed, A. R. Ajel, A. J. Humaidi, A. Alkhayyat, A. K. A. Mhdawi, Robust adaptive control of knee exoskeleton-assistant system based on nonlinear disturbance observer, *Actuators*, **11** (2022), 78. https://doi.org/10.3390/act11030078

23. G. Al Rezage, M. O. Tokhi, Fuzzy PID control of lower limb exoskeleton for elderly mobility, *2016 IEEE International Conference on Automation, Quality and Testing, Robotics (AQTR)*, Cluj-Napoca, Romania, 2016, 1–6. https://doi.org/10.1109/AQTR.2016.7501310

24. J. R. Meda-Gutiérrez, L. A. Zúñiga-Avilés, A. H. Vilchis-González, J. C. Ávila-Vilchis, Knee exoskeletons design approaches to boost strength capability: a review, *Appl. Sci.*, **11** (2021), 9990. https://doi.org/10.3390/app11219990

25. J. Zhou, S. Yang, Q. Xue, Lower limb rehabilitation exoskeleton robot: a review, *Adv. Mech. Eng.*, **13** (2021), 1–17. https://doi.org/10.1177/16878140211011862

26. X. Zhang, Z. Yue, J. Wang, Robotics in lower-limb rehabilitation after stroke, *Behav. Neurol.*, **2017** (2017), 3731802. https://doi.org/10.1155/2017/3731802

27. D. Shi, W. Zhang, W. Zhang, X. Ding, A review on lower limb rehabilitation exoskeleton robots, *Chin. J. Mech. Eng.*, **32** (2019), 1–11. https://doi.org/10.1186/s10033-019-0389-8

28. G. S. Sawicki, O. N. Beck, I. Kang, A. J. Young, The exoskeleton expansion: improving walking and running economy, *J. NeuroEng. Rehabil.*, **17** (2020), 1–9. https://doi.org/10.1186/s12984-020-00663-9

29. B. Kalita, J. Narayan, S. K. Dwivedy, Development of active lower limb robotic-based orthosis and exoskeleton devices: a systematic review, *Int. J. Soc. Robotics*, **13** (2021), 775–793. https://doi.org/10.1007/s12369-020-00662-9

30. D. Pinto-Fernandez, D. Torricelli, M. del Carmen Sanchez-Villamanan, F. Aller, K. Mombaur, R. Conti, et al., Performance evaluation of lower limb exoskeletons: a systematic review, *IEEE Trans. Neural Syst. Rehabil. Eng.*, **28** (2020), 1573–1583. https://doi.org/10.1109/TNSRE.2020.2989481

31. S. Jenhani, H. Gritli, J. Narayan, LMI-based robust composite position control of a knee rehabilitation exoskeleton robot subject to motion constraints, *Int. J. Dyn. Control*, **13** (2025), 115. https://doi.org/10.1007/s40435-025-01623-8

32. H. Rifaï, S. Mohammed, W. Hassani, Y. Amirat, Nested saturation based control of an actuated knee joint orthosis, *Mechatronics*, **23** (2013), 1141–1149. https://doi.org/10.1016/j.mechatronics.2013.09.007

33. R. Sharma, P. Gaur, S. Bhatt, D. Joshi, Optimal fuzzy logic-based control strategy for lower limb rehabilitation exoskeleton, *Appl. Soft Comput.*, **105** (2021), 107226. https://doi.org/10.1016/j.asoc.2021.107226

34. R. E. Skelton, Linear matrix inequality techniques in optimal control, In: J. Baillieul, T. Samad, *Encyclopedia of systems and control*, London: Springer, 2020. https://doi.org/10.1007/978-1-4471-5102-9_207-2

35. K. Z. Liu, LMI approach to robust control, In: J. Baillieul, T. Samad, *Encyclopedia of systems and control*, Springer International Publishing, Cham, 2021, 1152–1158. https://doi.org/10.1007/978-3-030-44184-5_161

36. C. Velandia, H. Celedón, D. A. Tibaduiza, C. Torres-Pinzón, J. Vitola, Design and control of an exoskeleton in rehabilitation tasks for lower limb, *2016 XXI Symposium on Signal Processing, Images and Artificial Vision (STSIVA)*, Bucaramanga, Colombia, 2016, 1–6. https://doi.org/10.1109/STSIVA.2016.7743341

37. J. Ibarra, K. Moussa, J. Lauber, Human torque estimation for an LMI-based convex control rehabilitation strategy using assistive robots, *2024 American Control Conference (ACC)*, Toronto, ON, Canada, 2024, 4889–4894. https://doi.org/10.23919/ACC60939.2024.10644226

38. R. Gaino, M. R. Covacic, R. Cardim, M. A. Sanches, A. A. De Carvalho, A. R. Biazeto, et al., Discrete takagi-sugeno fuzzy models applied to control the knee joint movement of paraplegic patients, *IEEE Access*, **8** (2020), 32714–32726.

39. Y. C. Huang, H. Hu, C. H. Chen, Y. J. Chen, K. C. Chi, Assistive robot design for lower limbs rehabilitation using fuzzy control, *Int. J. Fuzzy Syst.*, **23** (2021), 2384–2395. https://doi.org/10.1007/s40815-021-01152-4

40. M. Chen, X. Luo, X. Wang, H. Liu, Y. Mo, TS fuzzy-model-based tracking control of lower limb exoskeleton rehabilitation robot, *2024 IEEE International Conference on Cybernetics and Intelligent Systems (CIS) and IEEE International Conference on Robotics, Automation and Mechatronics (RAM)*, Hangzhou, China, 2024, 81–86. https://doi.org/10.1109/CIS-RAM61939.2024.10673013

41. M. Munadi, M. S. Nasir, M. Ariyanto, N. Iskandar, J. D. Setiawan, Design and simulation of PID controller for lower limb exoskeleton robot, *AIP Conf. Proc.*, **1983** (2018), 060008. https://doi.org/10.1063/1.5046300

42. N. Touati, I. Saidi, H. Ben Hadj Mbarek, PID control of a lower limb rehabilitation exoskeleton, *Przegl. Elektrotech.*, 2024.